Chapter

Synthesis of Supported Mesoporous Catalysts Using Supercritical CO_2

Soledad Guadalupe Aspromonte, Federico Andrés Piovano, Esther Alonso and Alicia Viviana Boix

Abstract

Metal and metal oxide nanoparticles have attracted increased attention due to their unusual physical and chemical properties. The nature, dispersion, and size of the nanoparticles are key factors in determining the activity and selectivity of the supported catalysts. Supercritical fluid deposition (SCFD) is a promising method to deposit metallic nanoparticles and films on inorganic porous supports. CO_2 is the most commonly used supercritical fluid (sc-CO_2) for material synthesis because it is nontoxic, nonreactive, nonflammable, and inexpensive. This work presents the synthesis of cobalt, nickel, and ruthenium nanoparticles on MCM-41, Al-MCM-41, MCM-48, and activated carbon supports in sc-CO_2. Batch and continuous deposition are studied, with two high-pressure reactor configurations: column or alternative (sandwich). To avoid the length of the bed being too long, the reagents were separated into smaller amounts and placed alternately, keeping the total mass of the precursor and support constant. The prepared samples were characterized by scanning electron (SEM/EDX) and transmission electron microscopy (TEM).

Keywords: metal, ruthenium, cobalt, nickel, supercritical fluids

1. Introduction

The chemical industry is partially responsible for the environmental problems caused by many of its processes, such as air pollution due to emissions produced by the incineration of fossil fuels. Thus, Green Chemistry emerges in response to these issues [1, 2]. This represents a constant motivation for the design of new processes that minimize the use of dangerous substances and the generation of polluting agents, maintaining the feature of the final product.

In this context, industrial processes should be designed to generate substances that are slight or not harmful to human health and the environment and, if it is possible, to use auxiliary agents (e.g., solvents) that are innocuous or with low toxicity. According to this dogma, in recent years, several investigations have been carried out involving the replacement of solvents used in many industries by other reaction media such as ionic liquids [3–5] or supercritical fluids (SCFs) [6–8].

Micro- and mesoporous materials are solid materials widely used in heterogeneous catalysis, due to their involvement in numerous reactions of industrial interest.

The deposition of metallic active phases on these substrates is of utmost importance in order to maintain the textural and structural properties and achieve good dispersion.

In this chapter, the study of supercritical carbon dioxide (sc-CO_2) as a solvent to deposit metallic nanoparticles (Ni, Co, Ru) on microporous (activated carbon) and mesoporous substrates (MCM-41 and MCM-48) is presented.

Supercritical fluid technology satisfies the principles of Green Chemistry, because it is a reagent with low toxicity and whose critical parameters are easily accessible and, therefore, energy consumption is minimized. In addition, through its compression it can be recovered, thus avoiding its release into the atmosphere. The combination of all these aspects, together with its good transport properties, as will be discussed in detail below, makes sc-CO_2 an excellent resource for developing new environmentally friendly technologies.

2. Supercritical fluids (SCFs)

A supercritical fluid (SCF) is defined as the state of a substance whose pressure and temperature are higher than their critical values [9]. In this state, the phase boundary between the liquid and the gas is interrupted at the critical point, which implies the formation of a homogeneous phase as observed in **Figure 1**. Therefore, it is possible for a substance to cross from the liquid to gaseous state passing through the supercritical region, without any phase transition (**Figure 2**).

Supercritical fluids have properties that are in many aspects unique and change considerably from those corresponding to the liquid or gaseous state of origin. Basically, SCFs have intermediate properties between those that characterize a liquid and those of a gas [10]. The thermal conductivity of SCFs approximates that of liquids, indicating that they have better properties with respect to heat conduction [11]. SCFs tend to occupy the entire volume of the enclosure and do not present interfacial tension, a behavior similar to gases (**Table 1**). Similar to gases, the density of SCFs varies enormously with pressure and temperature, although densities very close to those of liquids are reached. Thus, the characteristic property of SCFs is the wide range of high densities that they can adopt depending on pressure and/or temperature conditions. This differentiates them from liquids that are practically incompressible and from gases that have very low densities. These properties make FSC an effective medium for incorporating metals into porous solids.

Figure 3 presents the isotherms for a fluid, indicating the variation in density with pressure. It is noted that, above the critical point, there is only one phase and for high densities, the curve remains flat, indicating large variations in density for small increases in pressure.

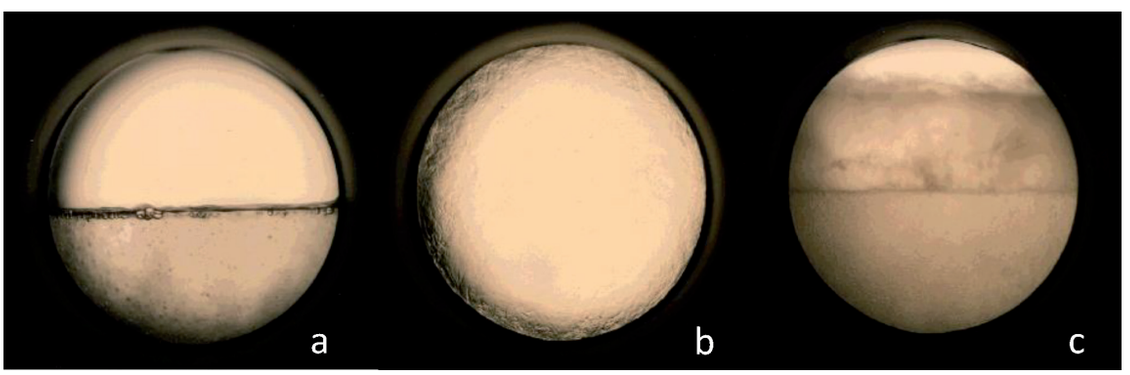

Figure 1.
Phases observed with a high pressure cell: (a) heterogeneous gas/liquid, (b) phase transition and (c) homogeneous in supercritical state.

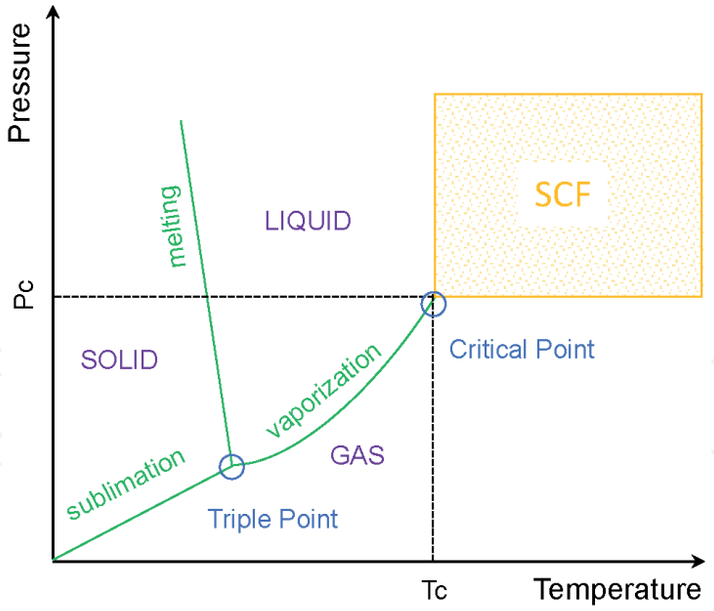

Figure 2.
P-T phase diagram.

Properties	Gas[a]	SCF[b]	Liquids[a]
Density ($kg \cdot m^{-3}$)	0.5–2.0	200–500	500–1500
Viscosity (mPa·s)	0.01–0.30	0.01–0.03	0.2–3.0
Diffusivity ($m^2 \cdot s^{-1}$)	10–5	10–7	10–9
Conductivity ($W \cdot m^{-1} \cdot K^{-1}$)	0.01–0.02	0.05–1.00	0.1–0.2

[a]*Properties at room temperatures.*
[b]*Properties close to critical point.*

Table 1.
Typical values for supercritical fluids (SCFs) [10].

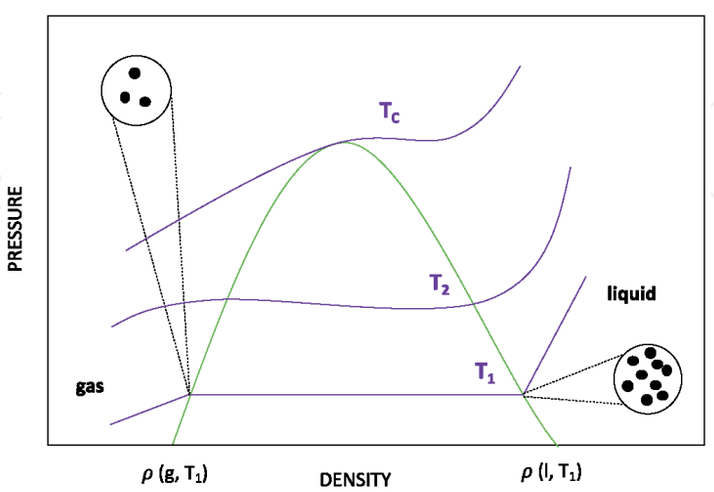

Figure 3.
Pressure-density diagram.

Therefore, considering the direct ratio that exists between fluid density and solvation power, SCFs can greatly vary their solvation capacity by small variations in pressure and/or temperature. Consequently, knowledge of the thermodynamic

properties of SCFs and their behavior near the critical point is essential for the proper design of separation reactions and processes.

Thus, the main applications of supercritical fluids are [12–14]:

- *Extraction*: leaves no residue; high purity extracts are obtained and do not require high temperatures.

- *Synthesis of materials*: SCFs allow obtaining solid materials with controlled properties, among which the obtaining of aerogels and the synthesis of ultrafine particles (nanoparticles) with very uniform morphology, high purity, and free of solvent residues can be highlighted.

- *Reaction medium*: the existence of a single phase allows optimal mass and energy transfer.

Indisputably, the most used supercritical fluid in research and industrial applications is carbon dioxide (CO_2). It is an innocuous, abundant, and inexpensive gas, with relatively low critical conditions (31°C and 71 bar) and therefore easy to operate.

Table 2 presents the temperature, pressure, and density conditions for different supercritical fluids [15].

2.1 Synthesis of materials in supercritical fluids

Currently, the material synthesis using SCFs represents a new area of research, particularly, in the field of nanoparticles. Polymeric materials, inorganic solids, and organic compounds, with uses in additives, medicines,

SCF	Name	T_c[a]	P_c[b]	ρ_c[c]
C_2H_4	Ethylene	9.3	50.4	220
Xe	Xenon	16.6	58.4	120
CO_2	Carbon dioxide	31.1	73.8	470
C_2H_6	Ethane	32.2	48.8	200
N_2O	Nitrous oxide	36.5	71.7	450
C_3H_8	Propane	96.7	42.5	220
NH_3	Ammonia	132.5	112.8	240
C_3H_8O	1-Propanol	235.2	47.6	270
CH_4O	Methanol	239.5	81.0	270
H_2O	Water	374.2	220.5	320
C_7H_8	Toluene	318.6	42.1	290
C_4H_{10}	n-Butane	152.0	38.0	228
C_5H_{12}	n-Pentane	196.6	33.7	232
C_6H_6	Benzene	289.5	49.2	300

[a]*Critical temperature (°C).*
[b]*Critical pressure (bar).*
[c]*Critical density (kg m^{-3}).*

Table 2.
Critical properties of different fluids.

pigments, cosmetics, biomaterials, optics, catalysts, or adsorbents, have been synthesized with supercritical fluids [16].

As a consequence, the development of various methods on the generation of particles with supercritical carbon dioxide (sc-CO_2) has grown rapidly in the last decades [17]. Among them, the rapid expansion of supercritical solutions (REES) is one of the most studied and used precipitation processes on an industrial and/or laboratory scale [18, 19]. This method involves the rapid expansion of a pressurized solution through a needle, causing extremely rapid nucleation of the solid solute in micronized form [20]. However, the rapid expansion of a supercritical solution in a liquid solvent (RESOLV) is an alternative to the REES technique [21]. In this case, expansion occurs in a liquid solvent instead of using sc-CO_2 to prevent particle aggregation [22].

However, FSCs can inhibit dissolution, thereby causing novel synthesis mechanisms, such as gas or supercritical anti-solvent (SAS) [23]. These procedures operate at high pressure and involve mixtures between an organic solution and a supercritical fluid [24]. As a consequence of high-pressure dissolution, the solution expands, and the solubility of the solute exhibits decrease rapidly. Finally, the mixture becomes supersaturated, and nanoparticles precipitate [25]. Similarly, particles of saturated gas solutions (PGSS) consist of dissolving a supercritical fluid in a solvent followed by rapid depressurization of this mixture through a nozzle that causes the formation of solid particles or liquid drops [26–29].

FSCs are also utilized in hydrothermal or solvothermal synthesis, participating through chemical reactions, such as hydrolysis and dehydration of solutions of metal salts in subcritical or supercritical water [30–32] or another solvent [33–35]. A novel recently synthesis technique is FSC microemulsion, in which water droplets in sc-CO_2 function as a micro-reactor [36–39].

Therefore, it is important to highlight one of the main advantages offered by technology with supercritical fluids. Through a simple change in operating conditions, it is possible to control the size and shape of the synthesized active phases. In this way it has been possible to produce a wide variety of materials, such as nanoparticles, powder coatings, films, core-shell particles, and nanocomposites.

Furthermore, it is complemented by certain organometallic complexes for the manufacture of different metals and metal oxides [40]. In the 1990s, several pioneering studies on the subject were reported [41–44] which subsequently led to the advancement and development of new processes, which can be summarized in the following fields:

- The use of organo-transition metal complexes as homogeneous catalysts for reactions in SCF and biphasic systems [45–48]

- Extraction of heavy metals from various matrices with SCF [49–51]

- Synthesis of inorganic powders with controlled size distribution by decomposition of organometallic complexes in SCF [52–56]

- Impregnation of polymers with different metal complexes and the subsequent transformation of the metal precursor within such matrices [57–62]

- Incorporation of metallic nanoparticles in porous inorganic and carbonaceous substrates by deposition of SCF [63–65]

This chapter focuses on the last point, in order to contribute to developing the incorporation of metallic active phases in porous substrates by dissolving organometallic complexes in sc-CO_2.

2.2 Supercritical fluid deposition

In recent years, the interest in nanostructured materials has grown enormously [66–69] due to the advantages they present in the area of heterogeneous catalysis. These are associated with its small size and, therefore, with its large specific surface.

In this way, several research studies have focused on improving the synthesis procedures of new catalytic materials, depositing metallic nanoparticles in porous materials (micro-, meso-, or macroporous), with high surface areas and uniform pore structures [70–74].

There are numerous techniques for incorporating metals on substrates, as well as for preparing supported metal films and/or nanoparticles, such as impregnation, coprecipitation, sol–gel, chemical vapor deposition, or microemulsions using organic stabilizing agents. All exhibit different advantages and disadvantages, but, in general, the main drawback of these synthesis methods is the control of the dimensions and dispersion of the particles, as well as the metallic content in the matrix of the support.

Reproducibility, size control, and stabilization under severe operating conditions are the most important challenges in the area of materials synthesis. In view of this, the use of supercritical fluids represents a promising synthesis method for the deposition of metallic nanoparticles on the solid surface and/or inside of porous substrates [75, 76]. Deposition with supercritical fluids (SCFD) is a very simple and ecological procedure [77, 78].

Reproducibility, size control, and stabilization under severe operating conditions are the most important challenges in the area of materials synthesis. In view of this, the use of supercritical fluids represents a promising synthesis method for the deposition of metallic nanoparticles on the surface of solids and/or within porous substrates.

Among SCFs, sc-CO_2 is the most widely used because it is abundant, inexpensive, nonflammable, nontoxic, environmentally benign, and easily accessible and leaves no residues that cannot be treated. Furthermore, it has a critical temperature (Tc) of 31°C and a critical pressure (Pc) of 71 bars.

In addition to the environmental benefits, sc-CO_2 has a high permeability index in almost all polymers, which makes it possible to incorporate metal precursors in various substrates. Furthermore, the dispersion of the particles, the diffusion rates in the substrate, and the separation of the SCF and the polymer chain of the metal of interest can be controlled through changes in temperature and pressure. These good sc-CO_2 properties have also been used in many applications such as separations (extraction and purification), chemical reactions, chromatography, drying of materials, and the synthesis of nanostructured materials [79, 80].

The SCFD technique involves three main stages (**Figure 4**) [81]:

i. Dissolution of the metallic precursor

ii. Adsorption and absorption of the metallic precursor in the support

iii. Reduction of the precursor to its metallic form

Thus, the first stage consists of dissolving an organometallic precursor using sc-CO_2 under optimal conditions to promote solubility in the medium: high pressure and moderate temperature. In the second phase, the resulting solution is exposed to the porous substrate with its subsequent adsorption on the support matrix, which represents the impregnation itself. Then the metal complex can be converted to its metal form as shown in **Figure 4**. Finally, the system decompresses slowly and

Figure 4.
Schematic diagram for supercritical fluid deposition method. (a) Organometallic precursor, (b) reducing agent, and (c) metal nanoparticles.

gradually until reaching atmospheric pressure. In this way, solvent residues and pore collapse are avoided, the very common difficulties in techniques for preparing catalysts.

The conversion of the adsorbed metal complex into metal nanoparticles can be carried out by different procedures. The conventional method is heating in an inert or hydrogen atmosphere, which can even be done before depressurization in the supercritical fluid phase.

Supercritical fluid reactive deposition (SCFRD) is a term used to refer to the case where metal reduction is performed in the synthesis process [82]. This technique is based on promoting the precipitation of metallic nanoparticles and their consequent deposition and growth on the pore while the organic part of the precursor remains dissolved in the sc-CO_2 and is released together with the gas [66, 83]. In this context, there are two possible ways: (i) injection of a reducing agent, such as H_2 or an alcohol, or (ii) a heat treatment to cause decomposition of the precursor. Consequently, this single-stage process for the synthesis of catalysts makes it possible to reduce operating times compared to other conventional techniques.

2.2.1 Dissolution of the metallic precursor in sc-CO_2

Dissolving the metal precursor in the supercritical phase is the first step in the deposition method. The metallic precursors can be organometallic or inorganic compounds, which will depend on the FSC used in the deposition. In particular, organometallic compounds have significant miscibility in SCFs such as sc-CO_2 and have been extensively used in SCFD techniques. In the case of inorganic precursors such as salts, they only show appreciable solubility in the case of critical and supercritical water [83].

The solubility and behavior of the precursor-SCF phase are very important parameters, since the adsorption of the precursor on the support depends on the concentration in the fluid phase. Some studies on the solubility of organometallic complexes in sc-CO_2 have been reported in the literature. From the point of view of solubility in sc-CO_2, the organometallic complexes can be diketones, dithiocarbamates, macrocycles, organophosphate reagents, hydroxamic acid, and other organic complexes. The organometallic precursors commonly used in the preparation of supported nanocomposites using SCFD are seen in **Table 3**.

2.2.2 Adsorption of the metallic precursor in the support

One of the most important aspects of the technique for preparing supported metals so that the particles are dispersed within the matrix is the absorption of the organometallic precursor in the substrate in the presence of SCF.

Similarly, in the event that the particles must be located on the surface of the support, the adsorption of the organometallic precursor on the surface in the presence of SCF plays an important role. Therefore, the study of the kinetics and

	β-Ketones	β-Fluored ketones	Cyclic ligands
Co			$Co(cp)_2$
Ni			$Ni(cp)_2$
Cu	$Cu(acac)_2$	$Cu(hfac)_2$	
	$Cu(tmhd)_2$	Cu(hfac)	
	$Cu(tmod)_2$		
Ru	$Ru(acac)_3$		$Ru(cod)(tmhd)_2$
Rh	$Rh(acac)_2$		Rh(cod)(acac)
Pd	$Pd(acac)_2$	$Pd(hfac)_2$	PdMe(cp)
Ag		Ag(cod)(hfac); Ag(hfac)(hmte) Ag(hfac)(tegme)	
Pt	$Pt(acac)_2$		$Pt(cod)me_2$
Ir			Ir(cp)(cod)me
Au	$Au(acac)me_2$		

acac—acetylacetonate; cod—1,5-cyclooctadiene; cp—cyclopentadienyl; hfac—hexafluoroacetylacetonate; hmte—hexamethyltriethylene; me—methyl; tegme—tetraethylene glycol dimethyl ether; tmhd—tetramethylheptadionate; tmod—trimethyloctanedione.

Table 3.
Summary of the organometallic precursors used in SCFD [83].

thermodynamics of the absorption and desorption processes is beneficial for the development of this technology.

The resistance to mass transfer on the outer surface of the particle and/or diffusion within the particle governs the kinetics of adsorption or absorption. In the first case, the resistance is quantified by the external mass transfer coefficient of the precursor, while, in the second case, it is a combination of the coefficient of diffusion of the fluid in the pores and of the diffusion of the solute adsorbed on the surface of pores. In absorption, the diffusion of the precursor into the SCF has to be considered when the matrix is full.

3. The importance of catalytic support

Like with metals, choosing a suitable support is a key aspect of catalyst design. The main role of a catalytic support is to fix and disperse the active centers, typically small metal particles or metal oxides, that participate in the reaction of interest. To maximize their efficiency, it is crucial to facilitate close contact between the reactive molecules with the nanoparticle-based surface atoms.

From these postulates, great efforts are made by several research groups to synthesize and optimize chemically stable support synthesis routes, with high and optimal surface areas to disperse active metallic phases.

Due to the high cost of certain metal catalysts such as noble metals, on an industrial scale, small particles with a good distribution and high surface/volume ratio are required.

Although the effective dispersion does not depend on the metal-support interaction, it is known that the morphology and physicochemical characteristics of the supports produce significant effects and can influence the catalytic activities. Carbonaceous materials, alumina and silica, are the commonly used catalytic supports.

3.1 Mesoporous supports

The main difference of mesoporous materials with zeolites is that the walls of their pores are not crystalline because they are made of amorphous silica, which does not have order at the atomic level. Thus, the order of these materials is related to the arrangement of the pores. Mesoporous materials have been studied as possible substitutes for zeolites, although their surface is also polar and they do not have the acidity of zeolites since they do not contain aluminum cations [84]. In addition, the size of their pores is greater than 2 nm, which means that there is no selectivity of form or present intra-particle diffusion problems [85].

Among the most studied mesoporous solids, a breakthrough originated in 1992 when the Mobil Research and Development Corporation published the synthesis of a series of mesoporous silicates that they designated as the M41S family. The main porous solids in this family are named MCM-41, MCM-48, and MCM-50 [Mobil Composition of Matter (MCM)] [86, 87]. The solid MCM-50 has an unstable lamellar structure, while the MCM-48 has a porous cubic metastable structure, which consists of two independent tri-directional channel systems (**Figure 5**).

The structure of MCM-41 silica is made up of a well-defined hexagonal network of unidirectional cylindrical pores, which provides the material with a high specific surface area (~1000 $m^2\ g^{-1}$) and a high pore volume [88, 89].

In general terms, the synthesis of these solids is carried out through the interaction between an inorganic phase and another micellar phase of an organic nature. The precursor agents of the structure or surfactants (templates) are characterized by being molecules with an amphiphilic character or also called "amphipathic molecules." In other words, they have a hydrophilic end (soluble in water) and a hydrophobic end (rejects water), which is usually a hydrocarbon chain. Like any other surfactant, they form micelles when in aqueous solution under certain conditions because they have a hydrophobic and a hydrophilic chain that cannot be separated. The surfactant micelles serve as templates or molds and create the internal porosity of the solid.

The micellar arrangement, responsible for the structuring of the final material, was attributed to the presence of surfactant molecules in an aqueous medium, under certain conditions of temperature, pH, and concentration, forming ordered structures known as liquid crystals [90].

The mechanism of formation of mesoporous materials is generally carried out through the sol-gel process, which has a number of advantages over others such as low temperature and homogeneity at the molecular level.

This method usually involves the hydrolysis and condensation of the precursors, which can be metal alkoxides or inorganic or organic salts. Furthermore, organic or

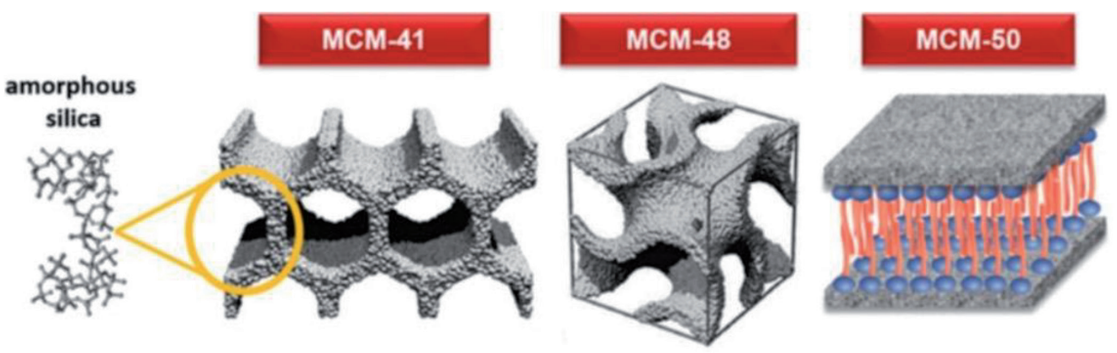

Figure 5.
Members of the M41S family. Adapted from [161].

aqueous solvents are used to dissolve the precursors. Occasionally, other substances are used to promote hydrolysis and condensation reactions [91]. Normally, the alkoxide groups are chosen in a sol-gel synthesis process as the silicon source. The reactivity of the chosen precursors largely depends on the degree of charge transfer and the ability to increase their coordination number.

Hydrolysis and condensation reactions are multistep processes, occurring sequentially, in parallel, and may be reversible. Condensation results in the formation of metal oxides or hydroxides, often with attached or attached organic groups. These organic groups may be due to incomplete hydrolysis or introduced as non-hydrolysable organic ligands [92].

The dimension and size of the pore system are dictated by the dimension and size of the micelles in solution. In the case of the hexagonal MCM-41 material, the pore diameter is between 20 and 40 Å when the length of the alkyl chain in the surfactant varies between C8 and C16. Finally, by calcination, excess surfactant is removed.

The siliceous walls of these materials do not have any order and are full of structural defects resulting from the hydrolysis of the silica source and its subsequent condensation. This condensation is not complete, so silicon atoms remain attached to OH– groups on the walls, called silanol groups.

3.1.1 Synthesis of mesoporous support

In general terms, the synthesis of mesoporous solids is carried out through the interaction between an inorganic phase and another micellar phase of an organic nature. The precursor agents of the structure (surfactants or templates) have a hydrophilic end (soluble in water) and a hydrophobic chain (rejects water), which is usually a hydrocarbon chain. Generally, these two parts tend to separate if added to a mixture with other substances, which cannot be fulfilled because both ends are joined by a chemical bond.

3.1.1.1 MCM-48

This support was prepared using a conventional hydrothermal method. For that, n-hexadecyltrimethylammonium bromide (2 g) was used as template [$CH_3(CH_2)_{15}N(Br)(CH_3)_3 \geq 98\%$, Sigma-Aldrich], ammonium hydroxide to condition the basic medium (13 cm^3, 20% as NH_3), and absolute ethanol as solvent (18 cm^3). The subsequent solution was stirred for 15 min, and the tetraethylorthosilicate (TEOS) was added such as Si source. It is necessary that TEOS were added dropwise to avoid the quick condensation. Then, the solution was further stirred for 18 hours at 30°C. Afterward, the white precipitate was collected by filtration, washed with distilled water, and dried at 60°C overnight.

Finally, the template was removed by calcination with a heating rate of 2°C min^{-1} at 550°C and maintained at 550°C for 8 hours in airflow.

3.1.1.2 MCM-41

The mesoporous substrates MCM-41 and AlMCM-41 were synthesized in a spherical way. For this, the commercial reagents that were used were the following:

- Surfactant: n-hexadecyltrimethylammonium bromide (C_{16}TMABr)
- Silicon source: tetraethyl orthosilicate (TEOS)
- Aluminum source: sodium aluminate ($NaAlO_4$)

- Ethanol (EtOH)

- Ammonium hydroxide solution (NH_4OH) 29% v/v

Thus, 1 g of C_{16}TMABr was dissolved in 19.2 ml of water at room temperature and continuous stirring. Then 24 g of absolute ethanol and 5.9 g of NH_4OH solution were added. Subsequently, 1.88 g of TEOS was added dropwise, to avoid rapid condensation of the Si source.

Ethanol is added to the preparation because it acts as a solvent, while water is a reagent for the hydrolysis reaction of TEOS. Ammonium hydroxide is used to achieve an alkaline medium and thus obtain discrete support particles. The mixture was kept under continuous stirring for 18 hours at 25°C. The resulting solid has the following molar composition:

$$\text{TEOS:0.3 } C_{16}\text{TMABr:11 } NH_3\text{:144 } H_2O\text{:58 EtOH}$$

The AlMCM-41 sample was prepared similarly to the MCM-41 solid. The difference is the addition of 0.04 g of sodium aluminate before adding TEOS, with the ratio Si/Al = 20.

The final solid was obtained by vacuum filtration, with subsequent washes until neutral pH was reached. Then, the samples were dried for 24 h at 80°C, and, finally, they were calcined in airflow at 5°C min^{-1} up to 550°C to achieve the total elimination of the surfactant.

4. Metals in catalysis and their applications

The area of heterogeneous catalysis is constantly developing, establishing innovative synthesis methods and modern metal deposition techniques, creating original supports, or trying to discover the necessary physicochemical properties of the catalyst for each reaction.

In this context, noble metal-based catalyst systems exhibit high activities for most reactions and are commonly used in numerous industrial applications. The main problem with the use of noble metals as the active phase is that, despite acting as an inert reaction, over time they deactivate due to poisoning with contaminating substances, coke deposition, or leaching of the active phases.

From this perspective, the development and extensive use of catalysts based on non-noble metals, such as Ru, Co, and Ni, are considered to be preferred from an industrial point of view, mainly for economic reasons.

4.1 Cobalt-based catalysts

In heterogeneous catalysis, cobalt represents one of the most studied active phases for decades. In particular, 2700 tn Co(0) are used annually as a homogeneous or heterogeneous catalyst in petrochemicals or plastic industries. Cobalt is used in the production of ultra-resistant resins or plastics for different purposes.

In addition, Co is used for the production of alcohols and aldehydes and consequently obtaining detergents. The active species can be metallic, cobalt oxide, hydroxide, or ionic.

On the other hand, there are numerous articles that report the behavior of cobalt-based catalysts applied in a wide variety of reactions of industrial significance. Those involving the breaking of C–H and C–C bonds at low temperatures are important. In this sense, cobalt catalysts supported on zirconia, ceria, and alumina

have reported high catalytic activity, similar to that obtained with the noble metal [93–96]. These solids have also been used satisfactorily in the dry-steam reforming process [97] in order to obtain synthesis gas enriched with hydrogen.

Llorca [98] demonstrated that the dispersion and reducibility of the cobalt species together with the cobalt-support interaction have important effects on the catalytic performance, being the key parameters in the stability and selectivity of the process. In order to improve efficiency, the synergistic effect of cobalt with other metals such as Ni [99–101], Ru [102, 103], and Fe or Cu [104] is also investigated.

Furthermore, there is a large group of research that focus on developing new materials for the Fischer-Tropsch synthesis (FTS) [105–107]. In order to efficiently obtain hydrocarbon mixtures from syngas (CO_2 and H_2) derived from coal, natural gas, or biomass resources, cobalt-based catalysts are widely used in this type of process due to their selectivity towards long-chain paraffin and strong resistance to deactivation and because they are economically viable. The nature and structure of the catalytic support, as well as the dispersion of Co(0) metal sites and the reducibility of cobalt species, directly influence the FTS performance. As a consequence, several synthesis strategies have been studied in recent years.

In this context, in order to achieve a high dispersion of surface active cobalt species, in some cases metal-support interaction is to stabilize the catalyst. Therefore, different supports have been studied such as titanium or magnesium oxides, zeolites, mesoporous silica (MCM-41 and SBA-15) [106, 108, 109], and carbon nanostructures (CNFs, MWCNTs, and CSc) [105, 110].

However, a strong interaction with the support can also decrease reducibility by creating nonreducible Co species such as $CoAl_2O_4$ and $CoTiO_3$. For this reason, some noble metal promoters, such as Pt, Re, or Ru [111, 112], are used to optimize the reduction of cobalt oxides and to inhibit coke deposition during FTS.

Although these are the best-known application processes, there are other examples where promising developments are taking place.

Unsupported cobalt catalysts showed good activity for ammonia synthesis [113, 114], improving thermal stability when cerium or barium were incorporated as promoters.

On the other hand, there is great scientific and environmental interest in reducing or eliminating NO_x emissions from combustion gases by means of selective catalytic reduction (SCR-NO_x). Cobalt catalysts supported on zeolites (MFI or FER) showed an increase in catalytic activity directly related to metal charge [115, 116].

In this sense, great efforts are made to develop new catalysts based on Co and applied in the combustion of volatile organic compounds (VOCs) generated by industry, transports, and residential/service sector [117–119]. To this point, high catalytic yields have been reported for the VOC oxidation at low temperatures given by cobalt oxides such as Co_2O_3 and Co_3O_4. This carries considerable environmental and economic benefits compared to traditional thermal oxidation.

4.1.1 Deposition of cobalt using sc-CO_2

Hunde and Watkins [120] were pioneers in the synthesis of cobalt and nickel on native silicon oxide using supercritical fluids. They also reported on the formation of Si-supported TaN and TiN films, without the need for a catalytic layer, by direct reduction of H_2 present in the cobaltocene ($CoCp_2$). For this, it was operated at a reduction temperature of cobaltocene in the range between 285 and 320°C and a pressure between 22.0 and 26.0 MPa. No significant deposition below 280°C was observed.

4.2 Nickel-based catalysts

Nickel-based catalysts are widely used due to their high activity at room temperature, leading to participation in the competitiveness of several industries.

The most important applications of this active phase include artificial fibers, vehicles parts, and nylon production. Adipic acid and caprolactam are obtained from the process of transforming benzene into cyclohexane using a nickel-based catalyst [121].

Also, a large part of the production of oils and fats derived from natural sources and used as food products (palm and vegetable oils) depends on the utilization of nickel catalysts. Fertilizer production involves technological processes with nickel catalysts for the ammonia production.

However, its main application is in oil refining. Raney Ni catalyst is widely used in hydrodenitrogenation to reduce NO_X and hydrodesulfurization to decrease SO_X concentration so that it is possible to obtain concentrations of these pollutants with levels lower than those legally required.

In addition to these applications, nickel catalysts supported on aluminum and porous silica represent the preferred option for cracking and hydroprocessing due to their ability to adsorb large amounts of hydrogen, which increases the efficiency of the reactions. It is important to note that nickel is less expensive relative to other metals like platinum.

Another field of application is in the production of synthesis gas as an alternative to the use of fossil fuels. One of those production methods is the reforming with liquefied natural gas [122, 123], ethanol [124], or an aqueous fraction of bio-oil [125, 126]. Nickel catalysts showed a good yield towards hydrogen production at a considerably lower cost than other noble metals in both fixed-bed and fluidized-bed reactors. However, these catalysts have the disadvantage of being deactivated significantly due to carbon deposition and sintering due to extremely severe operating conditions, leading to loss of active surface. For these reasons, there are continuous studies seeking to solve this problem facing it from different perspectives: the use of promoters (Zn, Mg, Zr, others [124, 126]), oxide supports (SiO_2 or Al_2O_3 [123, 127]), and different recuperation treatments [128].

Nevertheless, the most attractive process for syngas production is the CO_2 reforming of CH_4 or dry reforming (DRM) and all the side reactions also catalyzed by nickel.

These types of catalysts are replacing noble metals, such as Ru, Rh, and Pt, with DRM due to their availability and profitable viability. But, once again, its use is limited due to its high tendency to coke deposition and consequent deactivation. Side reactions, including CH_4 cracking [129], lead to the generation of carbonaceous deposits [130]. Furthermore, the endothermic nature of the reaction indicates that it is necessary to operate at high temperatures, tending to metal sintering. In this regard, the main parameters to be taken into account to reduce coke formation and improve catalytic performance have been studied and published, such as the nature of the support [131–133], the catalyst preparation method [134, 135], and the presence of modifiers [136, 137].

At the same time, among the growing concern over the depletion of fossil fuel reserves and environmental pollution, the generation of hydrogen from renewable resources such as biomass is emerging as an attractive alternative to energy demands. The use of nickel catalysts in the biomass gasification process cannot only increase H_2 yield but also decrease reactor size as a result of optimizing the reaction rate. Due to the same difficulties mentioned above, various catalytic supports, such as alumina, silica, and magnesium, were developed with metallic additives to improve thermal stability like Rh, Ru, Co, Fe, and Cu [138, 139].

Another instance is CO_2 methanation, developed by Sabatier and Senderens [140], which was industrialized in 1970 thanks to the use of catalysts, mainly Rh, Ru, or Pd. Recently, several supported nickel-based catalysts have been tested with high selectivity towards methane and a relatively low price [141, 142].

In addition, there are several articles and patents [143, 144] on the use of nickel as a catalyst for the hydrogenation of organic compounds, due to its ability to mainly hydrogenate C═C double bonds, carbonyl groups (aldehyde and ketone), nitro, nitrile, and oxime.

4.2.1 Deposition of nickel using sc-CO_2

Up to now, there are few articles related to the deposition of Ni nanoparticles by SCFD on micro- and mesoporous supports.

Peng et al. [145] have shown that $NiCp_2$ hydrogenolysis can take place by means of a low temperature autocatalyzed process (<70°C) in sc-CO_2 in both carbon nanotubes and flat surfaces.

In this sense, Bozbag et al. [146] reported the synthesis of Ni/AC, using activated carbon and $Ni(acac)_2$ as a precursor. The sc-CO_2 was used at 30 MPa and 60°C, followed by a heat treatment using H_2 at atmospheric pressure, achieving metallic loads of up to 6.5 wt.% with an average nanoparticle size around 10 nm.

Similarly, Taylor et al. [147] prepared Ni catalysts supported on carbon nanotubes and aluminosilicates with sc-MeOH and $Ni(acac)_2$, obtaining higher metal loads (60–70 wt.%). These were used in the production of hydrogen through the gasification of biomass in supercritical water.

Finally, the formation of a $NiCp_2$ film on Si, TaN, and TiN by means of chemical fluid at temperatures between 175 and 200°C and pressures from 19 to 23 MPa was reported [120]. The films were found to be essentially free of ligand-derived contamination, using a high-pressure cold-wall reactor and, therefore, restricting deposition only to heated substrates.

4.3 Ruthenium-based catalysts

Ruthenium is a transition metal that belongs to group VIII and has properties similar to those of the platinum. Ru-based catalysts can have a high potential in oxidative catalytic reactions such as asymmetric epoxidation of alkenes, dihydroxylation of olefins, or oxidative dehydrogenation of alcohols.

Ruthenium catalysts, mainly known industrially as Grubbs, are widely used in olefin metathesis reactions. They are widely applicable and requested due to their high tolerance to functional groups and stability [148, 149].

Similarly, in fine chemistry and pharmacy, Ru-based solids have been developed that facilitate hydrogen transfer. This alternative, which consists of adding hydrogen to a molecule from a source other than gaseous H_2 in the presence of a catalyst, is increasingly being used in the area of organic industry. On the other hand, ruthenium complexes are used in the reduction of ketones, aldehydes and imines to produce alcohols and amines, respectively [150, 151].

Many studies are trying to replace iron and other transition metals in reactions that require high temperature and pressure to achieve sufficient productivity. This can be seen in the synthesis of ammonia, for example, for which various ruthenium catalysts supported on $BaTiO_2$ [152] and carbon [153] have been tested.

In the energy field, a great deal of effort is devoted to finding materials that guarantee a safe and economical way to store hydrogen. Ruthenium-based catalysts are earning a significant place as a result of high yields. Akbayrak et al. [154, 155]

have reported that ruthenium supported on silica or nanotitania is one of the most active catalysts for the hydrogen generation from ammonia borane under mild conditions.

However, in general, most of the work focuses on hydrogenation reactions [156–158]. For example, in the industrial hydrogenation of benzene to obtain cyclohexane, nickel-based catalysts are used at temperature above 200°C and below 50 bars. These operating conditions lead to poor performance and promote undesired side reactions such as isomerization and hydrocracking, thus decreasing selectivity towards cyclohexane. In view of these arguments, numerous researchers are trying to replace this type of catalysts by others based on ruthenium alloys [156, 157].

Furthermore, as mentioned above, Raney nickel catalysts are used in the hydrogenation of glucose. However, new ruthenium-based catalysts are being developed due to their resistance to chemical attack [158, 159].

Increasingly, new types of ruthenium-based catalysts catalyze multiple hydrogenation reactions, even under severe operating conditions, such as transforming CO_2 into formic acid below 20–40 MPa and 80–150°C [160].

4.3.1 Deposition of ruthenium using sc-CO_2

There are some articles that study ruthenium deposition on different micro- and mesoporous supports using supercritical fluids. In this context, Yen et al. [161] showed the synthesis of Ru-MCM-41 solids using $Ru(cod)(thmd)_2$ as a precursor at 150°C, 10 MPa of CO_2, and 10 MPa of H_2. In this way, metallic nanoparticles are effectively distributed and dispersed with an average diameter of 3.4 nm. Likewise, Kim et al. [162] reported methods for preparing ruthenium nanodots on Si and HfO_2 films. In this case, $Ru_3(CO)_{12}$ was used as a precursor and dissolved in sc-CO_2 for 1 h, at 90°C and 23 MPa.

On the other hand, activated carbon is one of the most used catalytic supports in recent times. Due to this, there are numerous works that analyze the deposition of ruthenium on activated carbon [163–165] with sc-CO_2 and cosolvents such as methanol and ethanol. Operation variables such as temperature, pressure, and amount of cosolvent are optimized, being 45°C and 10 MPa the optimal conditions to obtain 2 wt.% of ruthenium.

5. Catalyst synthesis by SCFD

In this section, the supercritical fluid deposition will be developed for the synthesis of cobalt-, nickel-, and ruthenium-based catalysts on mesoporous supports using batch and continuous systems and detailing different configurations of the high-pressure reactor.

5.1 Batch device

The batch deposition experiments were carried out in a stainless-steel high-pressure vessel with an internal volume of 100 ml. The experimental setup operates up to 30 MPa pressure and 400°C maximum allowable working conditions (**Figure 6**).

A Milton Roy Dosapro metering pump (flow rate up to 6.2 L h^{-1} and a maximum pressure of 33 MPa) was used to supply the CO_2 to the reactor. The fluid is pre-cooled in a bath with an ethylene glycol/water (50/50) mixture cooled with an immersion cooler to ensure the liquid state of CO_2 for pumping.

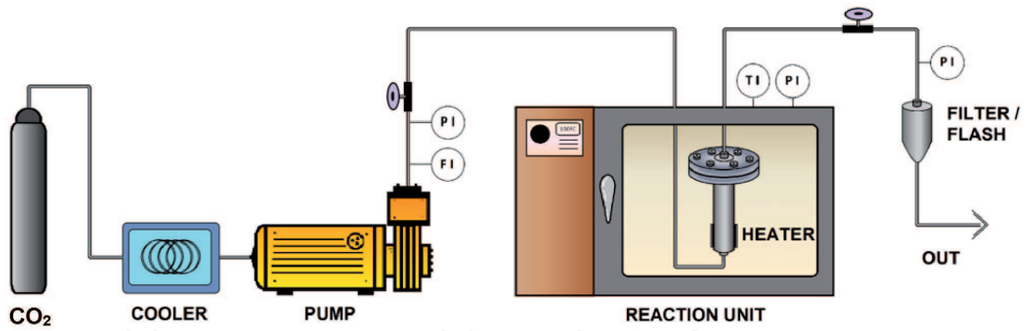

Figure 6.
Experimental device for the catalyst synthesis by batch SCFD.

Mass flow meter and a pressure gauge are installed in the pump outlet. The support and organometallic precursor are placed separated by a metal mesh to facilitate the circulation of sc-CO_2 and avoid its direct contact (**Figure 7**).

The reactor is equipped with two wall-mounted electrical resistors located to promote convective flow of sc-CO_2 and a K thermocouple.

During the first step, a precursor is dissolved by sc-CO_2 under optimal operation conditions to favor its solubility. Meanwhile, precursor adsorption onto the support from the medium takes place during the desired adsorption time. After this adsorption step, temperature is increased to 200°C to break down the organometallic compound, with its subsequent precipitation of the metallic nanoparticles during the desired decomposition time. Afterwards, the system is isochorically cooled down to subcritical conditions, and CO_2 is released from the reactor over a period approximately 30 min, which implies a slowly depressurization to atmospheric pressure to avoid drag metallic nanoparticles which are adsorbed over the support surface.

5.1.1 Mass transfer limitations

Due to the configuration of the experimental device, the synthesis process is carried out into the reactor without external stirring. To facilitate as far as possible the homogeneity of the solution, the electrical resistances are located at the bottom of the vessel, as it is shown in **Figure 7**, to favor the creation of convective currents.

Inside the high-pressure reactor, the support and precursor are located inside two glass vials separated by means of a wire mesh. The precursor is located in the lower part, and the support occupies the upper vial. This kind of configuration has been called "column" type.

Since the support is disposed as a fixed bed, it was decided to test whether all along the vial the same deposition was obtained or conversely there was some mass transfer limitation. For this reason, the metal content from the same sample was analyzed at three different heights. The results showed that there was a certain divergence, with a concentration gradient of up to 20% if the initial amount of support was too high, so a new configuration in the form of placing the reactants was contemplated in order to avoid the observed mass transfer limitations.

To avoid bed length which was too long, reagents were separated into smaller quantities in several vials and placed alternately, maintaining the total mass of both the precursor and support constant. This new configuration is called "sandwich," and a scheme of it is presented in **Figure 8**. The results are compared in **Table 4**.

Surprisingly, the improvement allows obtaining nanocomposites with really higher metallic loadings to 16 wt.%, showing that the "sandwich" configuration improves mass transfer in the system.

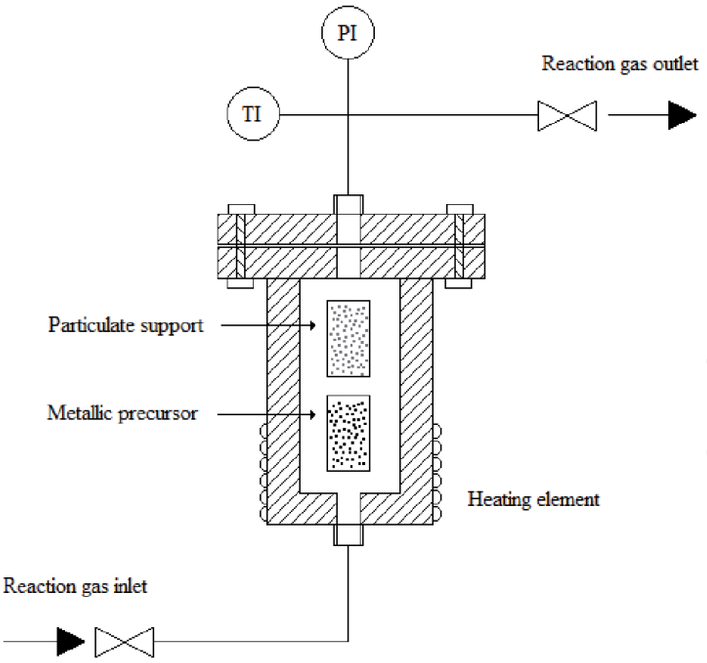

Figure 7.
Distribution of catalytic support and organometallic precursor within deposition chamber.

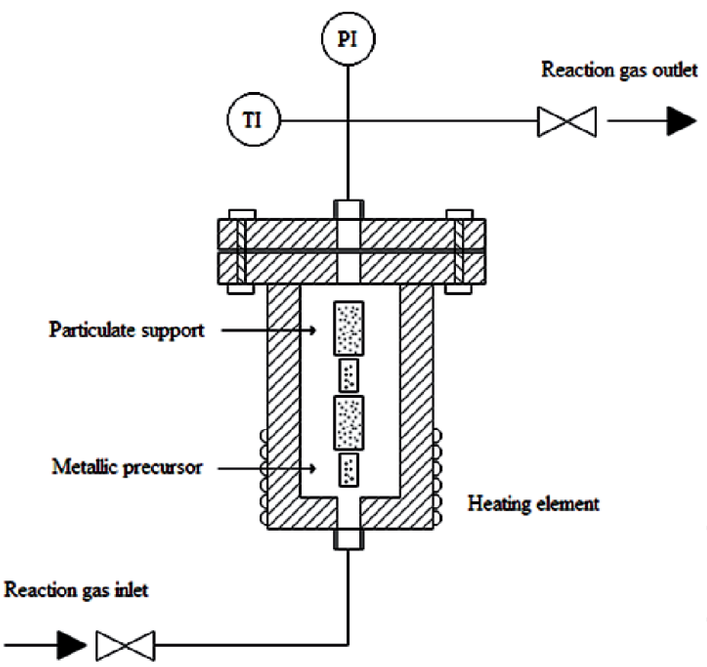

Figure 8.
Distribution of catalytic support and organometallic precursor in a "sandwich" configuration.

5.2 Continuous setup

The SCFD in continuous will be developed for synthesis of ruthenium-based catalysts. The continuous system is represented in **Figure 9**. CO_2 is pumped with a Jasco model PU-2080 Plus HPLC pump, which operates with a flow range between 1 μL to 10 ml min^{-1} and a maximum pressure of 22 MPa. The pump extraction line is cooled to guarantee the liquid state of the CO_2. So as to maintain a constant flow throughout the experiments, a mass flow meter controller with Bronkhorst Coriolis sensor calibrated to CO_2 combined with a controller model mini Cori-Flow (10–100 g h^{-1}) was established. In addition, a back-pressure valve is placed downstream of the reactor to control and manipulate the desired pressure. Finally, a Swagelok

Batches	wt.% Co	
	Column	Sandwich
1	3.2	5.8
2	4.4	13.7
3	6.0	16.6

Table 4.
Cobalt loading after each successive batch in column or sandwich configuration.

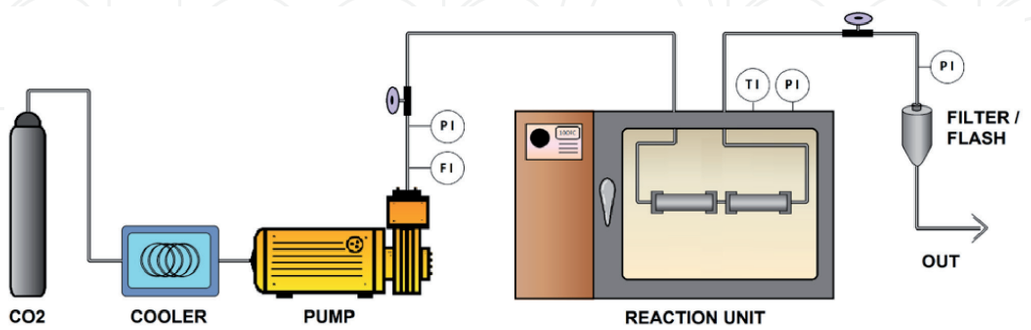

Figure 9.
Experimental device for the synthesis by SFRD in continuous mode.

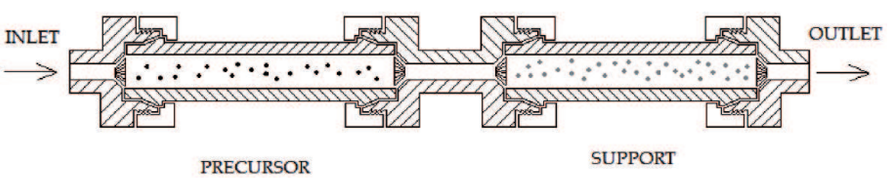

Figure 10.
Internal configuration of the high-pressure reactor in the continuous SCFD.

SS-4R3A relief valve is located to protect the system from overpressures, with a nominal pressure of up to 41 MPa at room temperature.

In this new configuration, the high-pressure container used in batch operation has been replaced by two sections located in horizontal position inside the furnace, as shown in **Figures 9** and **10**.

The first piece contains the organometallic precursor mixed with glass spheres to relief its dissolution into the CO_2 flow. Afterwards, the solution goes through the second tube, where the support is located.

The depositions were carried out under controlled conditions of pressure at 11 MPa and temperature at 60°C. The initial flow of CO_2 used (45 g h^{-1}) was sufficient to dissolve the precursor and be saturated before contact with the catalytic support. This premise was based on the observations made in the experiments carried out in the visual cell.

6. Metallic species deposited with sc-CO_2

6.1 Co-MCM-41 and Co-Al-MCM-41 catalysts

6.1.1 Physical, chemical, and textural properties

The adsorption and desorption experiments of N_2 at −196°C together with the measures of small-angle X-ray scattering (SAXS) were used to study the effect of

sc-CO_2 and the addition of Co on the hexagonal arrangement of the mesopores and pore size distribution in the prepared samples. **Figure 11** presents the N_2 adsorption/desorption isotherms obtained for the mesoporous support and the cobalt samples. All solids showed type IV adsorption isotherms, typical of mesoporous materials with a strong inflection at relative pressures $P/P_0 > 0.3$, indicating the uniformity of the mesopore size distribution.

Table 5 presents the quantitative results of N_2 adsorption and desorption for the samples with high and low cobalt content, which are compared with those obtained in their respective supports. In addition, the interplanar distance values d_{100} and unit cell parameter a_0 are shown, obtained by SAXS. The interplanar distance "d100," in the direction (1 0 0), was calculated using Bragg's law ($\lambda = 2 \cdot d_{hkl} \cdot \sin\theta$). Also, the unit cell parameter "a_0" was determined, which indicates the distance between the center of two adjacent pores in the hexagonal structure ($a_0 = 2 \cdot d_{100}/\sqrt{3}$) [166, 167]. Both parameters are included in **Table 5**, together with the average pore size of the synthesized samples, obtained from the BJH method.

The addition of aluminum to the MCM-41 support produces an approximate 38% of decrease in BET surface, while the average pore size remains relatively constant between 4.6 and 4.8 nm. On the other hand, beginning from the same amount of precursor, the Co content deposited in the Al-MCM-41 support is slightly higher than in the MCM-41 sample. It is known that the incorporation of Al to pure silica is done to give more acidity to the MCM-41 structure. Therefore, it is probably that there is a greater interaction as a consequence of the aluminum aggregate [92, 168].

Regarding the cobalt incorporation, the specific area decreases 9 and 20%, with the addition of 0.6 and 4.3 wt.% of Co to the MCM-41 support, respectively. On the other hand, the catalysts Co(0.8)-Al-MCM-41 and Co(5)-Al-MCM-41 show a decrease in the area of 7 and 12%, respectively. When the added Co content is high (4.3 and 5 wt.%), there is a slight decrease in the size of the porous cavities, as a consequence of the incorporation of Co inside the mesopores.

Consequently, to determine if cobalt incorporation affects the hexagonal arrangement of mesoporous channels, SAXS technique was used. In the case of amorphous materials such as MCM-41 and AlMCM-41, the regular arrangement or

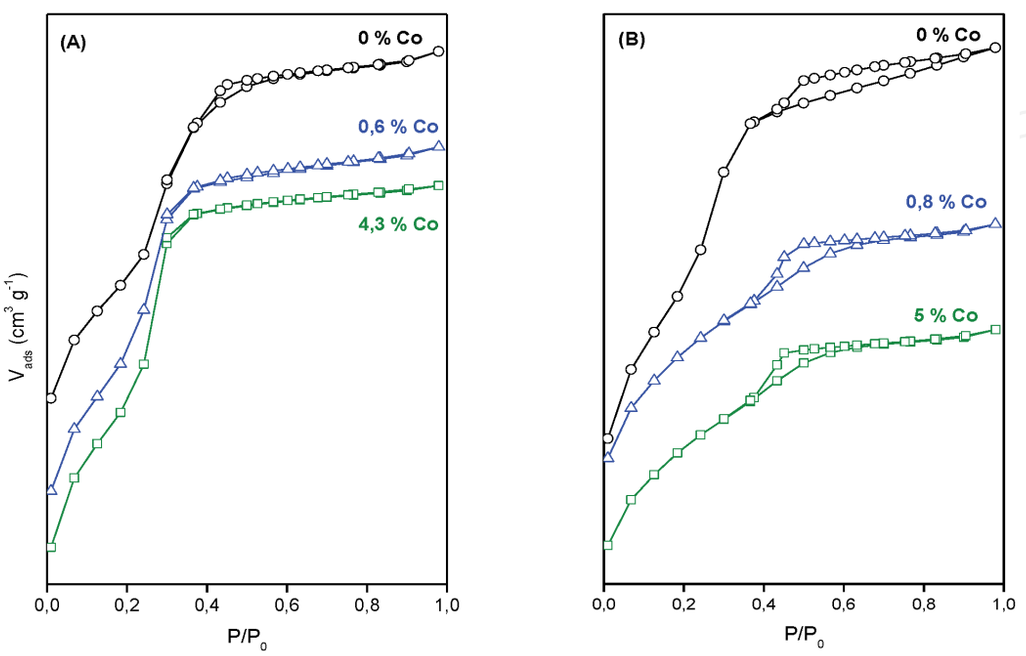

Figure 11.
Adsorption/desorption isotherms of N_2 at −196°C obtained for samples functionalized with Co on supports (A) MCM-41 and (B) Al-MCM-41.

Catalysts	% Co[a]	S_{BET} ($m^2 g^{-1}$)	v_p ($cm^3 g^{-1}$)	t_p[b]	d_{100}[c]	a_0[d]
MCM-41	0	1295	0.194	4.6	3.7	4.3
Co(0.6)	0.63	1183	0.173	4.5	3.7	4.3
Co(4.3)	4.34	1034	0.085	3.9	3.7	4.3
Al-MCM-41	0	807	0.216	4.8	3.7	4.3
Co(0.8)	0.82	752	0.198	4.1	3.4	3.9
Co(5)	5.10	709	0.156	3.9	3.4	3.9

[a]*Determined by ICP (wt.%).*
[b]*Average pore size (nm).*
[c]*Interplanar distance, $d_{100} = \lambda/2{\cdot}sen\ \theta$ (nm).*
[d]*Unit cell parameter, $a_0 = 11{,}547{\cdot}d_{100}$ (nm).*

Table 5.
Chemical, physical, and textural properties of co-mesoporous catalysts.

ordering of the pores produces reflections that appear as signals at low diffraction angles. The solids of the M41S family have easily identifiable diffractograms providing reflections (h k 0).

The results obtained by SAXS for the Co(x)-MCM-41 and Co(x)-Al-MCM-41 materials are presented in **Figure 12**. The appearance of an intense diffraction peak at 2.4° is characteristic of the (1 0 0) plane of the supports and indicates an ordered porous structure. In addition, there are other weaker diffraction peaks at 4.3 and 5.0° that correspond to the planes (1 1 0) and (2 0 0) and that verify the synthesized mesoporous structure.

As seen in **Figure 12A**, there are no notable changes in the shape and position of the diffraction peaks for the Co(x)-MCM-41 samples. On the other hand, when 5 wt.% of Co is deposited on the Al-MCM-41 substrate (**Figure 12B**), a slight shift of the main peak occurs towards higher diffraction angles (2θ = 2.6°). This suggests that the deposited cobalt charge causes a slight loss of the hexagonal arrangement. Furthermore, the cobalt incorporation in both mesoporous supports produces a decrease in the intensity of the diffraction peaks, which indicates the disorder of the hexagonal arrangement, but not breakage of the pores [87].

6.1.2 Morphology

Figure 13 presents the SEM images obtained after the addition of cobalt on supports MCM-41 and Al-MCM-41 with sc-CO_2 in batch conditions with "sandwich" reactor configuration (see **Table 4**).

It is observed that the procedure using supercritical fluids is a nonaggressive methodology, since the spherical morphology of the catalytic supports is maintained, with an average diameter close to 500 nm. Furthermore, it should be noted that the individual deposited nanoparticles cannot be detected directly using the secondary electron mode. However, when images are obtained through backscattered electron mode (BSE), areas of high electron density are observed, corresponding to cobalt particles. In **Figure 13**, brighter regions are highlighted, indicating areas of high electron density, due to the presence of cobalt. These zones are well dispersed and correspond to cobalt nanoparticles. Using EDX, cobalt concentrations close to 5.9 and 5.1 wt.% were obtained for the Co(4.3)-MCM-41 and Co(5)-Al-MCM-41 catalysts, respectively.

Figure 14 presents the mapping of SEM images from sample Co-MCM-41. Different shades in the gray scale are associated with various emission lines. In this

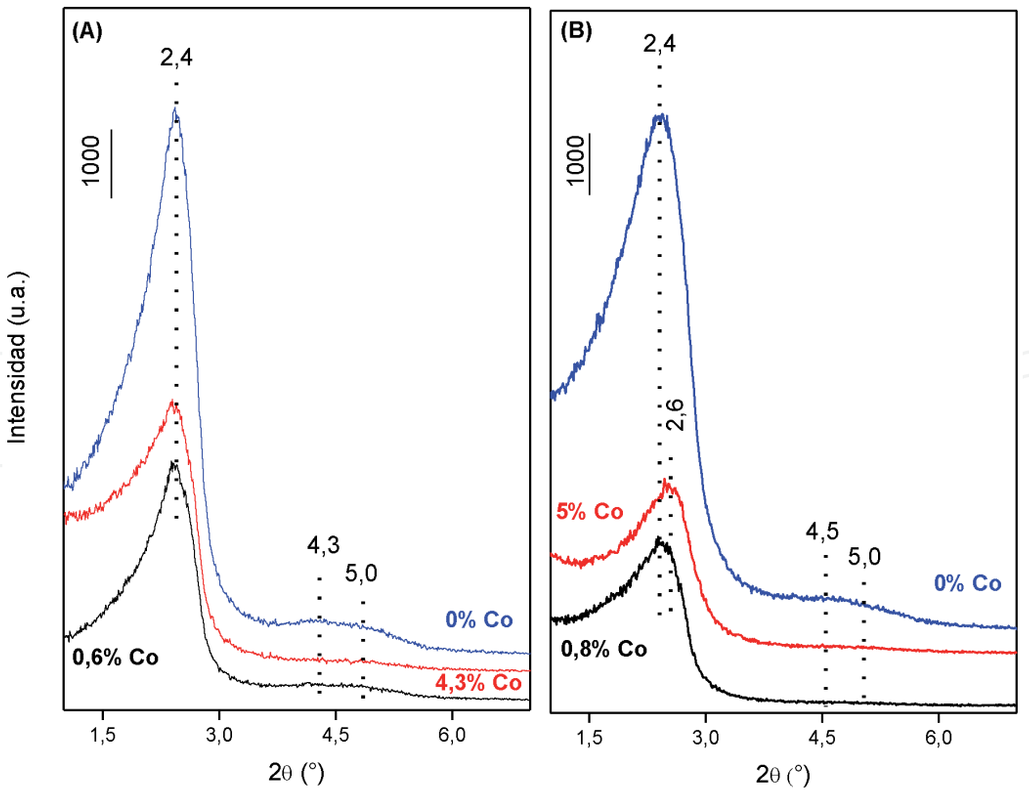

Figure 12.
Results obtained by SAXS for co-functionalized on supports (A) MCM-41 and (B) Al-MCM-41.

way, each tone in the image refers to the unique energy emission of the element of interest. When the cobalt charge was 4.3 wt.%, internal Co species and spherical nanoparticles were seen on the external surface of the MCM-41 substrate. When the concentration of cobaltocene (organometallic precursor) used was greater than the calculated solubility limit (0.336 g L^{-1}), the Co particles obtained had a diameter between 10 and 20 nm. Therefore, during the decomposition phase, the deposition of the nanoparticles occurs on the outer surface and inside the spherical particle of the support.

6.2 Ni-MCM-48 catalysts

6.2.1 Physical, chemical, and textural properties

The content of deposited nickel with sc-CO_2 was close to 3 wt.%, and it was determined by ICP. **Table 6** presents the surface and pore structure parameter of calcined MCM-48 and Ni-deposited catalyst. The BET surface area of the silica support MCM-48 is higher than the MCM-41, and this was 1641 m^2 g^{-1}. The pore volume and diameter were 0.9 cm^3 g^{-1} and 3.6 nm, respectively. After incorporating 3 wt.% Ni with sc-CO_2, the BET area and pore volume decrease close to 40.5%. The loss of textural properties is further accentuated compared to the catalyst with 5 wt.% Co. This can be associated with the fact that the ionic radius of nickel (0.78 Å) is higher than of Co (0.63 Å) and the solubility of nickel precursor (nickelocene) in sc-CO_2 is up to 1.5 times less than that of cobaltocene.

The N_2 adsorption/desorption isotherms (**Figure 15**) of the mesoporous MCM-48 and Ni-MCM-48 show the typical features of a mesoporous silica material, and it can be classified as type IV according to the IUPAC [169]. First, a sharp nitrogen uptake at P/P_0 in the range of 0–0.02 due to a monolayer adsorption on the walls of

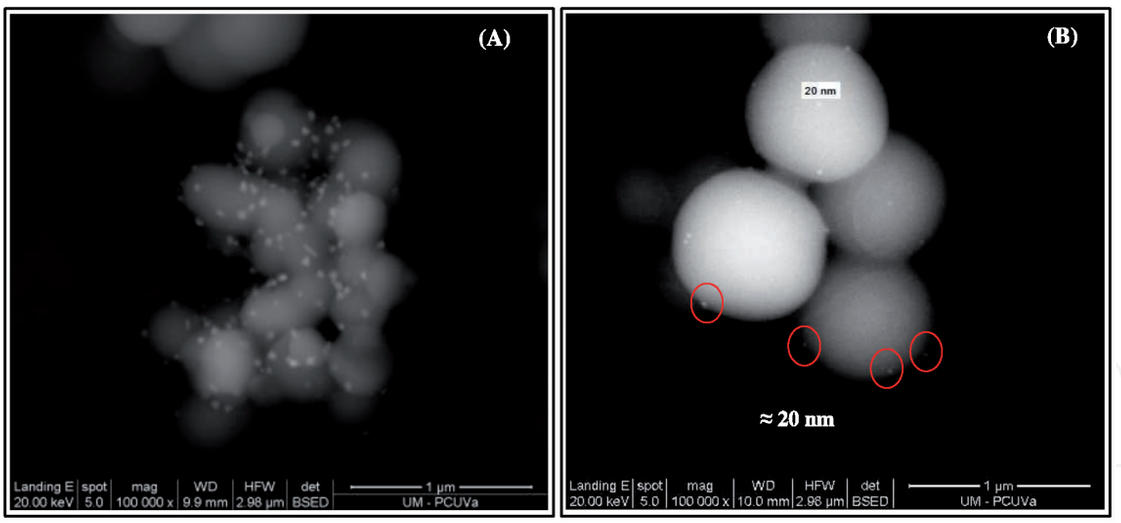

Figure 13.
SEM images obtained by backscattering of (A) Co-Al-MCM-41 and (B) Co-MCM-41.

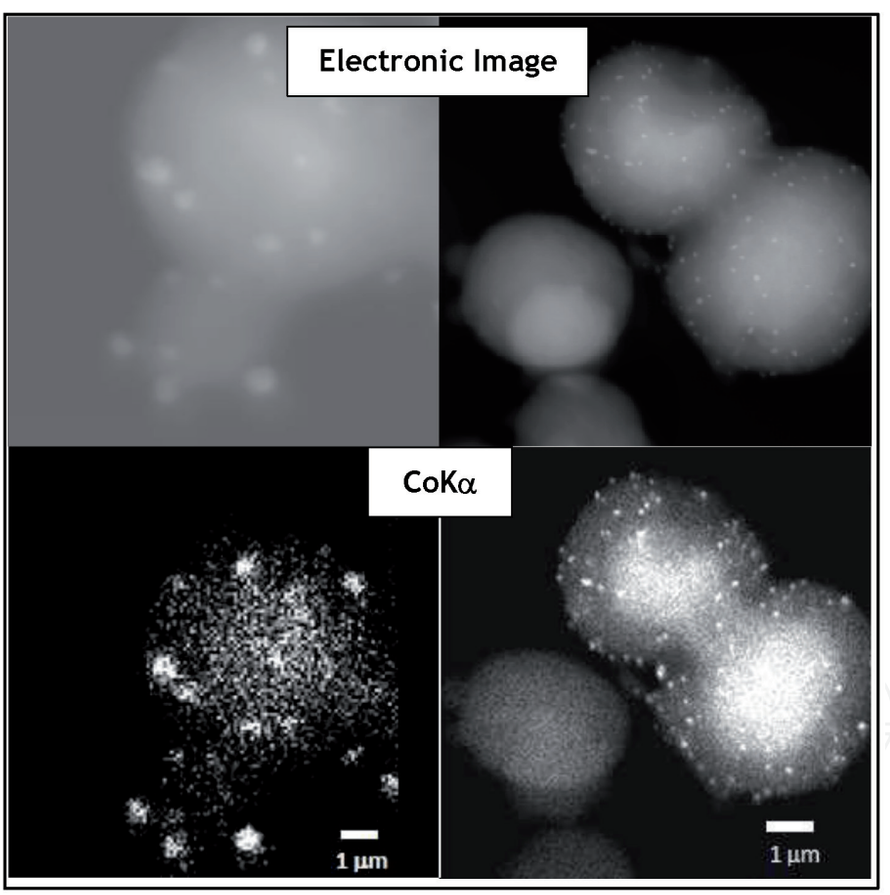

Figure 14.
Mapping of the SEM images obtained for the Co-MCM-41 catalyst.

Catalysts	% Ni[a]	S_{BET} ($m^2 \cdot g^{-1}$)	v_p ($cm^3 \cdot g^{-1}$)	t_p[b]
MCM-48	0	1641	0.90	3.6
Ni-MCM-48	3.0	977	0.45	1.4

[a] *Determined by ICP (wt.%).*
[b] *Average pore size (nm).*

Table 6.
Chemical and textural properties of Ni-MCM-48 catalyst.

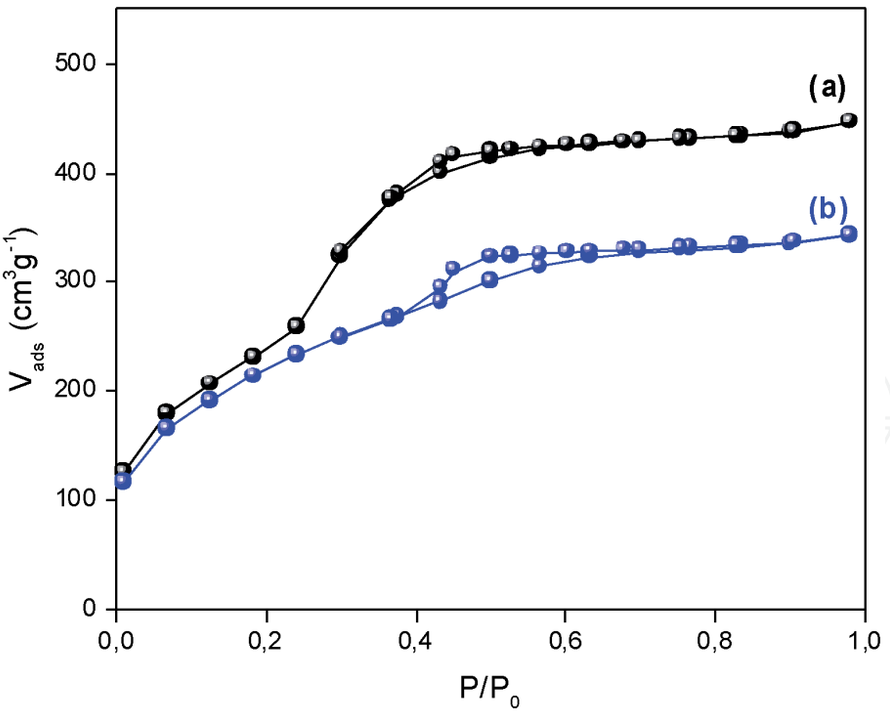

Figure 15.
Adsorption/desorption isotherms of N_2 at −196°C obtained for samples (a) MCM-48 and (b) Ni-MCM-48.

MCM-48 is observed. This step is followed by an abrupt increase in the volume of nitrogen adsorbed at P/P_0 in the range of 0.2–0.3 associated to capillary condensation of N_2 in the channels of MCM-48, suggesting uniformity of the channels and a narrow pore size distribution [170].

6.2.2 Morphology

Table 7 shows the results of nickel content after the impregnation by SCFD in batch conditions with column and sandwich reactor configuration.

The first three experiments were carried out under the same conditions: 14 MPa, 200°C, 1 h, and a reactor configuration in column. The nickel concentration in all of them was very similar, with an average value of 2.7 wt.% of nickel and a standard deviation lower than 0.1 wt.%, indicating the robustness of the SCFD process.

On the other hand, when studying the sandwich-type configuration of the reactor, in which several vials with precursor and support are placed alternately inside the reactor, they do not reveal a significant difference in the metallic charge as if it occurred with cobalt. Although depositions made in sequential charges have achieved increasing concentrations of metal, the rate of increase is considerably less from batch to batch, compared to cobalt. As observed in **Table 7**, the increase in nickel concentration after the second deposition is 52%, while it decreases to 14% after the third batch.

However, it is important to note that this type of configuration allows obtaining a greater amount of catalyst in a single operation.

In this way, it is observed that the SCFD method represents a valuable and versatile technology, with reasonable reproducibility, that can be adapted and applied to other metal-support systems with acceptable efficiencies.

Instead, an electron microscopy (SEM/TEM) was used in order to study the morphology and the dispersion of the nickel nanoparticles incorporated by SCFD in batch and sandwich configuration. In this sense, **Figure 16** shows spherical particles of support with an average diameter of about 200 nm and metallic nanoparticles dispersed on the surface.

Batches	wt.% Ni column	Batches	wt.% Ni sandwich
1	2.8	1	2.5
1	2.8	2	3.7
1	2.6	3	4.2

Table 7.
Nickel loading in batch with column or sandwich reactor configuration at 14 MPa, 200°C and 1 h.

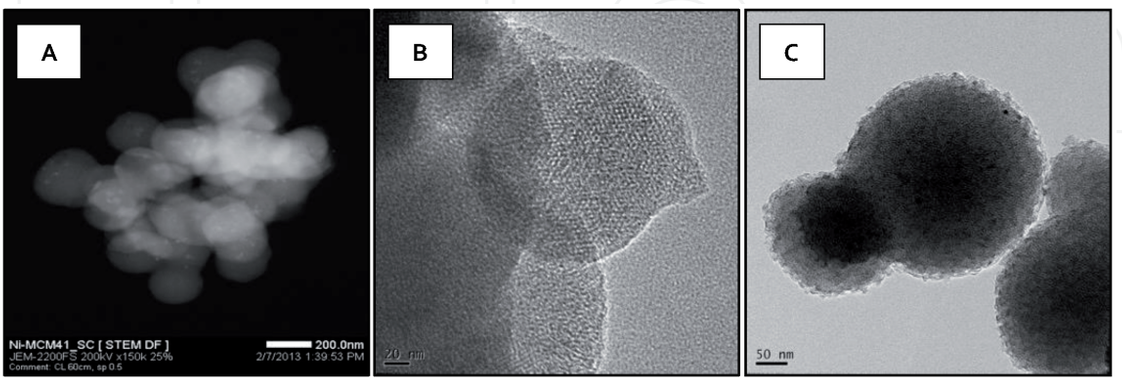

Figure 16.
TEM pictures of Ni-MCM-48 (A): BSE mode; (B and C) electronic image.

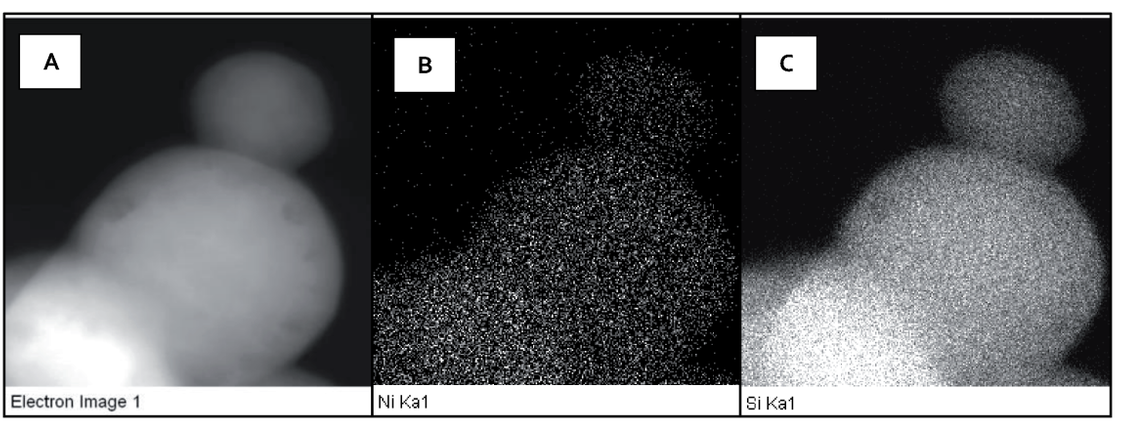

Figure 17.
Mapping of the SEM images obtained for the Ni-MCM-48 catalyst. (A) Electron image, (B) NiKα, and (C) SiKα spectra.

As occurred with the cobalt deposition, channels can be distinguished in **Figure 16**, which indicates that the high pressure of SCFD method does not modify the original structure of the support.

The distribution of the metal was observed by means of a mapping of the electron image (**Figure 17**). In these images, the homogenous distribution of the metal throughout the catalysts prepared by SCFD is observed, being perfectly distributed both surface and inside the support, without detecting any gradient of concentration or uncoated areas.

6.3 Ru-MCM-48 and Ru-C catalysts

6.3.1 Physical, chemical, and textural properties

Figure 18 shows the N_2 adsorption/desorption isotherms for the AC support and Ru-based catalysts. According to the IUPAC classification, the N_2 isotherms for AC

and Ru-AC catalysts are classified as type I. Generally, the microporous solids such as activated carbons and molecular sieve zeolites give type I isotherms [171].

The quantitative data obtained from the isotherms are presented in **Table 8**. The surface area obtained for the carbonaceous support was 794 $m^2\ g^{-1}$, while the average diameter and pore volume were 2.1 nm and 0.77 $cm^3\ g^{-1}$, respectively. By incorporating 4.3 wt.% Ru with supercritical CO_2, the textural properties remain practically constant, being the surface area of 739 $m^2\ g^{-1}$, the pore size of 2.0 nm, and the volume of 0.70 $cm^3\ g^{-1}$. This behavior would indicate that ruthenium was successfully incorporated into the carbonaceous matrix, with high dispersion without collapsing the microporous structure.

On the other hand, when the ruthenium content was increased to 8 wt.%, the surface area decreased 30% compared to the initial AC. Also, pore size and volume decrease 23 and 12%, respectively.

In this way, it is verified that the supercritical fluid technology allowed to incorporate up to 8 wt.% of Ru in a microporous carbonaceous support in a satisfactory way without significantly altering the textural properties of the same.

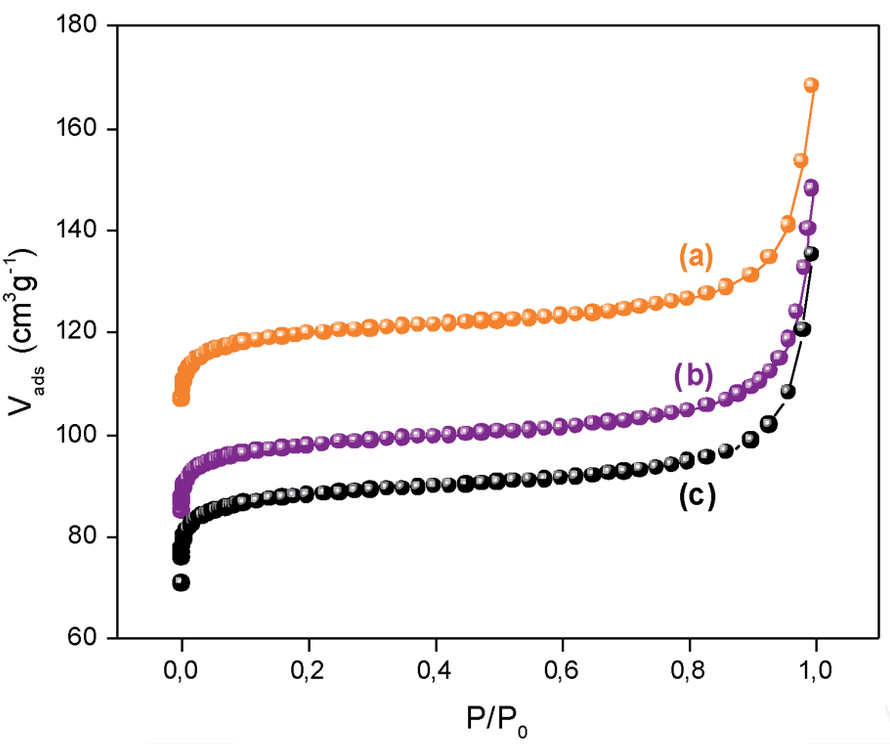

Figure 18.
Adsorption/desorption isotherms of N_2 at −196°C obtained for (a) AC support, (b) Ru(4.3)-AC, and (c) Ru(8)-AC catalysts.

Catalysts	% Ru[a]	S_{BET} ($m^2 \cdot g^{-1}$)	v_p ($cm^3 \cdot g^{-1}$)	t_p[b]
MCM-48	0	1641	0.90	3.6
Ru-MCM-48	3.0	977	0.45	1.4
AC	0	794	0.77	2.2
Ru(4.3)-AC	4.3	739	0.70	2.0
Ru(8)-AC	8	524	0.68	1.7

[a] *Determined by ICP (wt.%).*
[b] *Average pore size (nm).*

Table 8.
Chemical and textural properties of Ru-based catalysts.

Following the same line of research, when 4.7 wt.% Ru is incorporated into the MCM-48 mesoporous support, a 46% of decrease in the BET surface area is observed. Similar behavior shows the diameter and pore volume. This behavior was also observed with the incorporation of 3% Ni (see Section 6.2).

In this sense, it is observed that the modification of the textural properties of the synthesized catalysts depends on each particular case and factors like (i) the nature of the metal precursor used, (ii) the solubility of the precursor in sc-CO_2, and (iii) the incorporated metal content. Evidently, the optimized P and T conditions influence the solubility of the precursor but do not affect the structure of the catalytic supports.

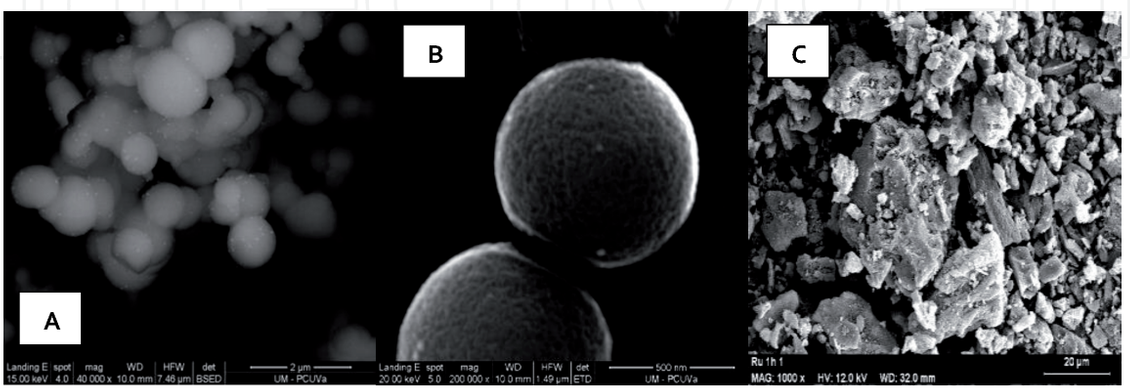

Figure 19.
SEM images of (A and B) Ru-MCM-48 and (C) Ru-C catalysts prepared by SCFD in continuous mode.

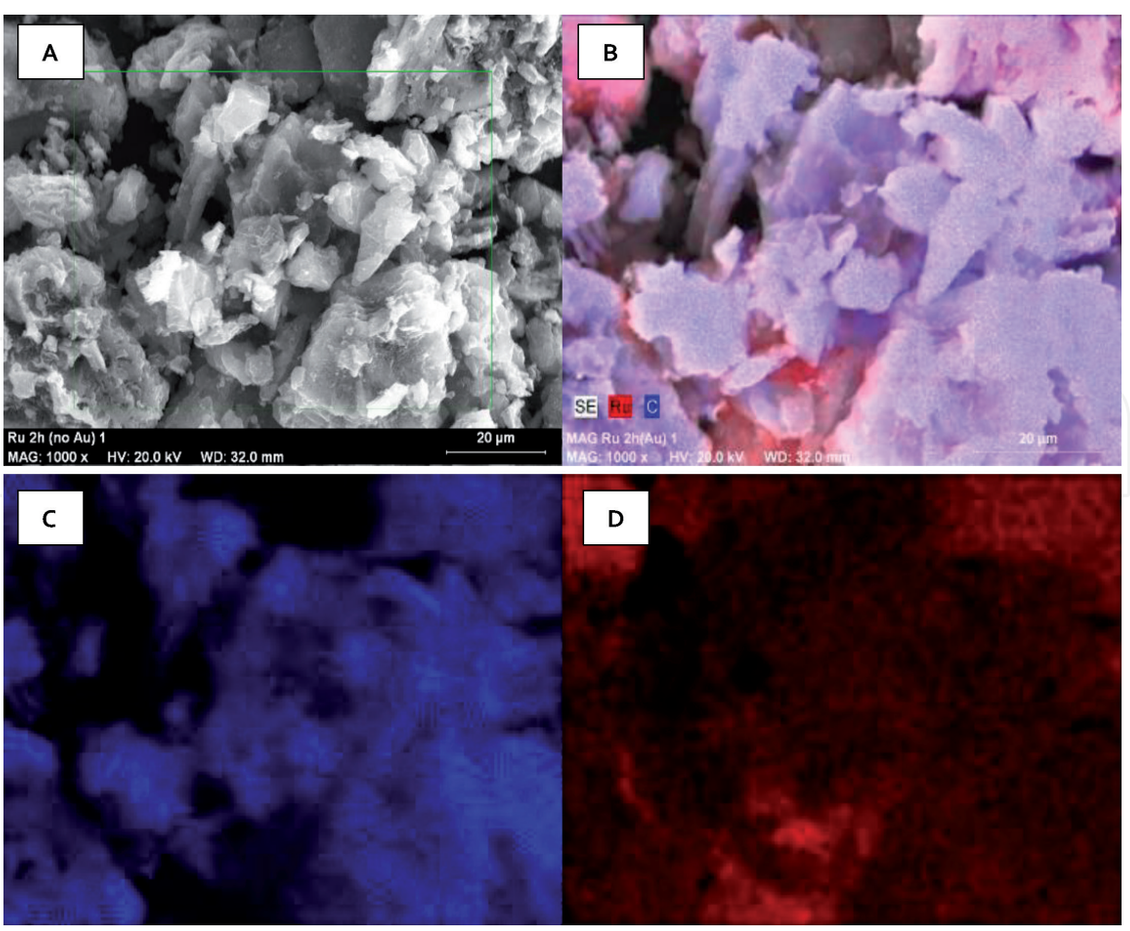

Figure 20.
Mapping of the SEM images obtained for the Ru-C catalyst. (A) Electron image, (B) SiKα, (C) CKα, and (D) RuKα spectra.

6.3.2 Morphology

Figure 19 presents the SEM images obtained after the addition of ruthenium on supports MCM-48 and activated carbon with sc-CO_2 in continuous conditions. Spherical particles with a size distribution between 200 and 500 nm were observed for MCM-48 support. Well-dispersed nanoparticles with an average diameter close to 10 nm were exposed on the MCM-48 surface (**Figure 19A** and **B**).

On the other hand, carbon active has a different morphology, irregularly shaped particles with very different sizes. **Figure 19C** presents the morphology corresponding to the Ru-C catalyst. From this SEM image, it is not possible to observe the deposited metal phase, so the mapping of the obtained electronic image was performed (**Figure 20**).

It is observed that the metal is completely deposited on the surface of the activated carbon with homogeneous distribution. Increasing the concentration of metal in the catalyst, it still maintains a uniform distribution, without finding gradient of concentration.

7. Conclusions

Supercritical CO_2 represents an optimal means to synthesize metallic nanoparticles (cobalt, nickel, or ruthenium) on substrates such as MCM-48, MCM-41, Al-MCM-41, and activated carbon.

It has important advantages over other conventional means of preparation, such as complete synthesis in a single stage, without the need for subsequent calcination or reduction. Furthermore, the synthesis process is simple, using CO_2 which is nontoxic, nonreactive, nonflammable, and inexpensive, with adequate pressure and temperature.

It is a process that can be performed in batch or continuous, optimizing the configuration of the reactor towards the sandwich arrangement of the support and organometallic precursor, thus obtaining a greater amount of catalyst in a single synthesis.

In this way, high metallic contents (close to 10%) are achieved with high dispersion and without significantly affecting the textural properties of the support.

Therefore, the effective deposition of different active phases on micro- and mesoporous substrates depends on each particular case and factors like the nature of the metal precursor used, the solubility of the precursor in sc-CO_2, and the incorporated metal content. Evidently, the optimized P and T conditions influence the solubility of the precursor but do not affect the structure of the catalytic supports.

Finally, reactive deposition with supercritical CO_2 represents an alternative for the reuse of CO_2 captured in other processes.

Acknowledgements

The authors acknowledge the financial support received from the Junta de Castilla y León, Spain (VA040u16), and from the Universidad Nacional del Litoral and CONICET, Argentina. They are also grateful to Santa Fe Agency of Science, Technology and Innovation (ASACTEI) for the financial support received through the Project 2017-00157.

Author details

Soledad Guadalupe Aspromonte[1*], Federico Andrés Piovano[1], Esther Alonso[2] and Alicia Viviana Boix[1]

1 INCAPE (FIQ, UNL-CONICET), Research Institute in Catalysis and Petrochemistry, Santa Fe, Argentina

2 High Pressure Processes Group, Department of Chemical Engineering and Environmental Technology, BioEcoUva, Research Institute on Bioeconomy, University of Valladolid, Valladolid, Spain

*Address all correspondence to: saspromonte@fiq.unl.edu.ar

References

[1] Poliakoff M, Fitzpatrick JM, Farre TR, Anastas PT. Green Chemistry: Science and politics of change. Science. 2002;**297**(5582):807-810. DOI: 10.1126/science.297.5582.807

[2] Anastas PT, Kirchhoff MM. Origins, currents status, and future challenges of Green Chemistry. Accounts of Chemical Research. 2002;**35**(9):686-694

[3] Yang Z, Pan W. Ionic liquids: Green solvents for nonaqueous biocatalysis. Enzyme and Microbial Technology. 2005;**37**(1):19-28

[4] Cho C-W, Jeon Y-C, Pham TPT, Vijayaraghavan K, Yun Y-S. The ecotoxicity of ionic liquids and traditional organic solvents on microalga *Selenastrum capricornutum*. Ecotoxicology and Environmental Safety. 2008;**71**(1):166-171

[5] Zhu P, Chen Y, Wang LY, Zhou M. Treatment of waste printed circuit board by green solvent using ionic liquid. Waste Management. 2012;**32**(10):1914-1918

[6] Nalawade SP, Picchioni F, Janssen LPBM. Supercritical carbon dioxide as a green solvent for processing polymer melts: Processing aspects and applications. Progress in Polymer Science. 2006;**31**(1):19-43

[7] Ramsey E, Sun Q, Zhang Z, Zhang C, Gou W. Mini-review: Green sustainable processes using supercritical fluid carbon dioxide. Journal of Environmental Sciences. 2009;**21**(6):720-726

[8] Machida H, Takesue M, Smith RL Jr. Green chemical processes with supercritical fluids: Properties, materials, separations and energy. The Journal of Supercritical Fluids. 2011;**60**:2-15

[9] McNaught AD, Wilkinson A. IUPAC Compendium of Chemical Terminology, the Gold Book. Oxford: Blackwell Scientific Publications; 2006

[10] Blackburn JM, Long DP, Cabañas A, Watkins JJ. Deposition of conformal copper and nickel films from supercritical carbon dioxide. Science. 2001;**294**:141-145

[11] Sotelo Sánchez JL, Ovejero Escudero G. Procesos con fluidos supercríticos. Anales de la Real Sociedad Española de Química. 2003;**4**:15-23

[12] Cansell F, Aymonier C. Review: Design of functional nanostructured materials using supercritical fluids. Journal of Supercritical Fluids. 2009;**47**:508-516

[13] Pai RA, Humayun R, Schulberg MT, Sebgupta A, Sun JN, Watkins JJ. Mesoporous silicates prepared using preorganized templates in supercritical fluids. Science. 2004;**303**:507-510

[14] Zhang J, Han B. Review: Supercritical CO_2-continuous microemulsions and compressed CO_2-expanded reverse microemulsions. Journal of Supercritical Fluids. 2007;**47**:179-186

[15] Reverchon E, Adami R. Review: Nanomaterials and supercritical fluids. Journal of Supercritical Fluids. 2006;**37**:1-22

[16] Knez Z, Markocic E, Leitgeb M, Primozic M, Knez Hrncic M, Skerget M. Industrial applications of supercritical fluids: A review. Energy. 2014;**77**:235-243

[17] Jung J, Perrut M. Particle design using supercritical fluids: Literature and patent survey. Journal of Supercritical Fluids. 2001;**20**:179-219

[18] Huang Z, Sun G-B, Chiew YC, Kawi S. Formation of ultrafine aspirin particles through rapid expansion of supercritical solution (RESS). Powder Technology. 2005;**160**(2):127-134

[19] Türk M, Bolten D. Formation of submicron poorly water-soluble drugs by rapid expansion of supercritical solution (RESS): Results for naproxen. The Journal of Supercritical Fluids. 2010;**55**(2):778-785

[20] Ovaskainen L, Chigome S, Birkin NA, Howdle SM, Torto N, Wagberg L, et al. Superhydrophobic polymeric coatings produced by rapid expansion of supercritical solutions combined with electrostatic deposition (RESS-ED). The Journal of Supercritical Fluids. 2014;**95**:610-617

[21] Baseri H, Lotfollahi MN. Formation of gemfibrozil with narrow particle size distribution via rapid expansion of supercritical solution process (RESS). Powder Technology. 2013;**235**:677-684

[22] Keshmiri K, Vatanara A, Tavakoli O, Manafi N. Production of ultrafine clobetasol propionate via rapid expansion of supercritical solution (RESS): Full factorial approach. The Journal of Supercritical Fluids. 2015;**101**:176-183

[23] Esfandiari N. Production of micro and nanoparticles of pharmaceutical by supercritical carbon dioxide. The Journal of Supercritical Fluids. 2015;**100**:129-141

[24] Wang H, Jiang H, Kuang L, Zhang M. Synthesis of highly dispersed MnOx-CeO_2 nanospheres by surfactant-assisted supercritical anti-solvent (SAS) technique. The important role of the surfactant. The Journal of Supercritical Fluids. 2014;**92**:84-92

[25] Adeli E. A comparative evaluation between utilizing SAS supercritical fluid technique and solvent evaporation method in preparation of azithromycin solid dispersions for dissolution rate enhancement. The Journal of Supercritical Fluids. 2014;**87**:9-21

[26] Cocero MJ, Martín Á, Mattea F, Varona S. Encapsulation and co-precipitation processes with supercritical fluids: Fundamentals and applications. The Journal of Supercritical Fluids. 2009;**47**(3):546-555

[27] Varona S, Kareth S, Martín Á, Cocero MJ. Formulation of lavandin essential oil with biopolymers by PGSS for application as biocide in ecological agriculture. The Journal of Supercritical Fluids. 2010;**54**(3):369-377

[28] Pestieau A, Krier F, Lebrun P, Brouwers A, Streel B, Evrard B. Optimization of a PGSS (particles from gas saturated solutions) process for a fenofibrate lipid-based solid dispersion formulation. International Journal of Pharmaceutics. 2015;**485**(1-2):295-305

[29] Bochon I, Kareth S, Kilzer A, Petermann M. Synthesis and powder generation of powder coatings using supercritical carbon dioxide. The Journal of Supercritical Fluids. 2015;**96**:324-333

[30] Ma CY, Liu JJ, Zhang Y, Wang XZ. Simulation for scale-up of a confined jet mixer for continuous hydrothermal flow synthesis of nanomaterials. The Journal of Supercritical Fluids. 2015;**98**:211-221

[31] Zhu K, Hu G. Supercritical hydrothermal synthesis of titanium dioxide nanostructures with controlled phase and morphology. The Journal of Supercritical Fluids. 2014;**94**:165-173

[32] Kawasaki S-I, Sue K, Ookawara R, Wakashima Y, Suzuki A, Hakuta Y, et al. Engineering study of continuous supercritical hydrothermal method using a T-shaped mixer: Experimental synthesis of NiO nanoparticles and CFD

simulation. The Journal of Supercritical Fluids. 2010;**54**(1):96-102

[33] Inoue M. Solvothermal synthesis of metal oxides. In: Somiya S, editor. Handbook of Advanced Ceramics. 2nd ed. Oxford: Academic Press; 2013. pp. 927-948

[34] Wang M, Chen C, Zhao B, Zeng Q, He D. Solvothermal synthesis of nanostructured TiO_2 photocatalyst in supercritical CO_2 fluids. Materials Letters. 2013;**109**:104-107

[35] Leng Y, Wang W, Zhang L, Zabihi F, Zhao Y. Fabrication and photocatalytical enhancement of ZnO-graphene hybrid using a continuous solvothermal technique. The Journal of Supercritical Fluids. 2014;**91**:61-67

[36] Malik MA, Wani MY, Hashim MA. Microemulsion method: A novel route to synthesize organic and inorganic nanomaterials: 1st nano update. Arabian Journal of Chemistry. 2012;**5**(4):397-417

[37] Blattner C, Zoumpanioti M, Kröner J, Schmeer G, Xenakis A, Kunz W. Biocatalysis using lipase encapsulated in microemulsion-based organogels in supercritical carbon dioxide. The Journal of Supercritical Fluids. 2006;**36**(3):182-193

[38] Shimizu R, Nibe A, Sawada K, Enokida Y, Yamamoto I. Preparation of hydrophobic platinum catalysts using a water-in-CO_2 microemulsion. The Journal of Supercritical Fluids. 2008;**44**(1):109-114

[39] Lu L, An X. Silver nanoparticles synthesis using H_2 as reducing agent in toluene-supercritical CO_2 microemulsion. The Journal of Supercritical Fluids. 2015;**99**:29-37

[40] Darr JA, Poliakoff M. New directions in inorganic and metal-organic coordination chemistry in supercritical fluids. Chemical Reviews. 1999;**99**(2):495-542

[41] Wenclawiak B, Bickmann F. Fluid and supercritical CO_2 as eluent in metal chelate chromatography. Analytical Chemistry. 1984;**319**:305-310

[42] Banister JA, George MW, Grubert S, Howdle SM, Jobling M, Johnson FPA, et al. Organometallic photochemistry in supercritical fluids: Reactions of cyclopentadienyl carbonyl and phosphine carbonyl complexes of manganese with dinitrogen. Journal of Organometallic Chemistry. 1994;**484**(1-2):129-135

[43] Lin Y, Smart NG, Wai CM. Supercritical fluid extraction and chromatography of metal chelates and organometallic compounds. TrAC Trends in Analytical Chemistry. 1995;**14**(3):123-133

[44] Bayona JM, Development of supercritical fluid extraction procedures for the determination of organotin compounds in sediment. In: Quevauviller EAM, Griepink B, editors. Techniques and Instrumentation in Analytical Chemistry. Netherlands: Elsevier BV; 1995. pp. 465-487

[45] Rathke JW, Klingler RJ, Krause TR. Propylene hydroformylation in supercritical carbon dioxide. Organometallics. 1991;**10**:1350-1355

[46] Dharmidhikari S, Abraham MA. Rhodium supported on activated carbon as a heterogeneous catalyst for hydroformylation of propylene in supercritical carbon dioxide. The Journal of Supercritical Fluids. 2000;**18**(1):1-10

[47] Bektesevic S, Kleman AM, Marteel-Parrish AE, Abraham MA. Hydroformylation in supercritical carbon dioxide: Catalysis and benign solvents. The Journal of Supercritical Fluids. 2006;**38**(2):232-241

[48] Koeken ACJ, de Bakker SJM, Costerus HM, van den Broeke LJP, Deelman B-J, Keurentjes JTF. Evaluation of pressure and correlation to reaction rates during homogeneously catalyzed hydroformylation in supercritical carbon dioxide. The Journal of Supercritical Fluids. 2008;**46**(1):47-56

[49] Laintz KE, Wai CM, Yonker CR, Smith RD. Extraction of metal ions from liquid and solid materials by supercritical carbon dioxide. Analytical Chemistry. 1992;**64**:28-75

[50] Liang M-T, Liang R-C, Lin C-H, Hsu P-J, Wu L-Y, Chen H-F, et al. Metal extraction of a spiked solid with supercritical carbon dioxide. The Journal of Supercritical Fluids. 2013;**79**:324-329

[51] Erkey C. Supercritical carbon dioxide extraction of metals from aqueous solutions: A review. The Journal of Supercritical Fluids. 2000;**17**(3):259-287

[52] Reverchon E, Adami R. Nanomaterials and supercritical fluids. The Journal of Supercritical Fluids. 2006;**37**(1):1-22

[53] Shah PS, Husain S, Johnston KP, Korgel BA. Nanocrystal arrested precipitation in supercritical carbon dioxide. Journal of Physical Chemistry. 2001;**105**:9433-9440

[54] Mezian IMJ, Pathak P, Beacham F, Allard LF, Sun Y-P. Nanoparticle formation in rapid expansion of water-in-supercritical carbon dioxide microemulsion into liquid solution. The Journal of Supercritical Fluids. 2005;**34**(1):91-97

[55] Haldorai Y, Shim J-J, Lim KT. Synthesis of polymer-inorganic filler nanocomposites in supercritical CO_2. The Journal of Supercritical Fluids. 2012;**71**:45-63

[56] Aymonier C, Loppinet-Serani A, Reverón H, Garrabos Y, Cansell F. Review of supercritical fluids in inorganic materials science. The Journal of Supercritical Fluids. 2006;**38**(2):242-251

[57] Higginbotham CL, Yons JGL, Kennedy JE. Polymer processing using supercritical fluids. In: Thomas S, Weimin Y, editors. Advances in Polymer Processing. Sawston, Cambridge: Woodhead Publishing; 2009. pp. 384-401

[58] Hussain YA, Grant CS. Ibuprofen impregnation into submicron polymeric films in supercritical carbon dioxide. The Journal of Supercritical Fluids. 2012;**71**:127-135

[59] Cooper AI, Kazarian SG, Poliakoff M. Supercritical fluid impregnation of polyethylene films, a new approach to studying equilibria in matrices; the hydrogen bonding of fluoroalcohols to $(\eta^5\text{-}C_5Me_5)Ir(CO)_2$ and the effect on C·H activation. Chemical Physics Letters. 1993;**206**(1-4):175-180

[60] Tomasko DL, Han X, Liu D, Gao W. Supercritical fluid applications in polymer nanocomposites. Current Opinion in Solid State and Materials Science. 2003;**7**(4-5):407-412

[61] Watkins JJ, McCarthy TJ. Polymer/metal nanocomposite synthesis in supercritical CO_2. Chemistry of Materials. 1995;**7**:1991-1994

[62] Bozbağ SE, Erkey C. Supercritical deposition: Current status and perspectives for the preparation of supported metal nanostructures. The Journal of Supercritical Fluids. 2015;**96**:298-312

[63] Erkey C. Preparation of metallic supported nanoparticles and films using supercritical fluid deposition. The Journal of Supercritical Fluids. 2009;**47**(3):517-522

[64] Caputo G, De Marco I, Reverchon E. Silica aerogel-metal composites produced by supercritical adsorption. The Journal of Supercritical Fluids. 2010;**54**(2):243-249

[65] Aspromonte SG, Sastre A, Boix AV, Cocero MJ, Alonso E. Cobalt oxide nanoparticles on mesoporous MCM-41 and Al-MCM-41 by supercritical CO_2 deposition. Microporous and Mesoporous Materials. 2012;**148**(1):53-61

[66] Alonso E, Montequi I, Lucas S, Cocero MJ. Synthesis of titanium oxide particles in supercritical CO_2: Effect of operational variables in the characteristics of the final product. The Journal of Supercritical Fluids. 2007;**39**(3):453-461

[67] Alonso E, Montequi I, Cocero MJ. Effect of synthesis conditions on photocatalytic activity of TiO_2 powders synthesized in supercritical CO_2. The Journal of Supercritical Fluids. 2009;**49**(2):233-238

[68] Bozbag SE, Sanli D, Erkey C. Synthesis of nanostructures materials using supercritical CO_2: Physical transformations. Journal of Material Sciences. 2012;**47**:2995-3025

[69] Bozbag SE, Sanli D, Erkey C. Synthesis of nanostructures materials using supercritical CO_2: Chemical transformations. Journal of Material Sciences. 2012;**47**:3469-3492

[70] Sinha Ray S. Applications, environmental impact and future development of environmentally friendly polymer nanocomposites (EFPNCs). In: Ray SS, editor. Environmentally Friendly Polymer Nanocomposites. Sawston, Cambridge: Woodhead Publishing; 2013. pp. 467-477

[71] Fitzgerald G, DeJoannis J, Meunier M. Multiscale modeling of nanomaterials: Recent developments and future prospects. In: Zhang VKT, editor. Modeling, Characterization, and Production of Nanomaterials. Sawston, Cambridge: Woodhead Publishing; 2015. pp. 3-53

[72] Pereira SR, Coelho MC. Can nanomaterials be a solution for application on alternative vehicles?—A review paper on life cycle assessment and risk analysis. International Journal of Hydrogen Energy. 2015;**40**(14):4969-4979

[73] Jiang K, Pinchuk AO. Noble metal nanomaterials: Synthetic routes, fundamental properties, and promising applications. In: Solid State Physics. Cambridge: Academic Press; 2015

[74] Wu R, Zhou K, Yue CY, Wei J, Pan Y. Recent progress in synthesis, properties and potential applications of SiC nanomaterials. Progress in Materials Science. 2015;**72**:1-60

[75] Zhang Y, Erkey C. Preparation of supported metallic nanoparticles using supercritical fluids: A review. The Journal of Supercritical Fluids. 2006;**38**(2):252-267

[76] Yen CH, Lin HW, Phan TD, Tan CS. Chemical fluid deposition of monometallic and bimetallic nanoparticles on ordered mesoporous silica as hydrogenation catalysts. Journal of Nanoscience and Nanotechnology. 2011;**11**(3):2465-2469

[77] Cangül B, Zhang LC, Aindow M, Erkey C. Preparation of carbon black supported Pd, Pt and Pd-Pt nanoparticles using supercritical CO_2 deposition. The Journal of Supercritical Fluids. 2009;**50**(1):82-90

[78] Garrido E, Aymonier C, Roiban L, Ersen O, Labrugère C, Gaillard P, et al. Noble metals supported on carbon nanotubes using supercritical fluids for the preparation of composite materials:

A look at the interface. The Journal of Supercritical Fluids. 2015;**101**:110-116

[79] Sanli D, Erkey C. Effect of polymer molecular weight and deposition temperature on the properties of silica aerogel/hydroxy-terminated poly(dimethylsiloxane) nanocomposites prepared by reactive supercritical deposition. The Journal of Supercritical Fluids. 2015;**5**(22):11708-11717

[80] Wolff S, Crone M, Muller T, Enders M, Bräse S, Türk M. Preparation of supported Pt nanoparticles by supercritical fluid reactive deposition: Influence of precursor, substrate and pressure on product properties. The Journal of Supercritical Fluids. 2014;**95**:588-596

[81] Müller S, Türk M. Production of supported gold and gold-silver nanoparticles by supercritical fluid reactive deposition: Effect of substrate properties. The Journal of Supercritical Fluids. 2015;**96**:287-297

[82] Kameo A, Yoshimura T, Esumi K. Preparation of noble metal nanoparticles in supercritical carbon dioxide. Colloids and Surfaces A: Physicochemical and Engineering Aspects. 2003;**215**:181-189

[83] Erkey C. Review: Preparation of metallic supported nanoparticles and films using supercritical fluid deposition. Journal of Supercritical Fluids. 2009;**47**:517-522

[84] Ciesla U, Schüth F. A review—Ordered mesoporous materials. Microporous and Mesoporous Materials. 1999;**27**:131-149

[85] Melero JA, Iglesias J, Moreno J. Chapter 12: Advanced metal-containing mesostructured silicas for novel catalytic applications. In: Mesoporous Materials: Properties, Preparation and Applications. NY: Nova Science Publishers; 2009

[86] Chen CY, Burkett SL, Li HX, Davis ME. Studies on mesoporous materials. II. Synthesis mechanism of MCM-41. Microporous Materials. 1993;**2**:21-34

[87] Beck JS, Vartuli JC. Recent advances in the synthesis, characterization and applications of mesoporous molecular sieves. Current Opinion in Solid State & Materials Science. 1996;**1**:76-87

[88] Zhou W, Klinowski J. The mechanism of channel formation in the mesoporous molecular sieve MCM-41. Chemical Physics Letters. 1998;**292**:207-212

[89] Taguchi A, Schüth F. Ordered mesoporous materials in catalysis—Review. Microporous and Mesoporous Materials. 2005;**77**:1-45

[90] Trong On D, Desplantier-Giscard D, Danumah C, Kaliaguine S. Perspectives in catalytic applications of mesostructured materials—A review. Applied Catalysis A: General. 2001;**222**:299-357

[91] Luechinger M, Frunz L, Pirngruber GD, Prins R. A mechanistic explanation of the formation of high quality MCM-41 with high hydrothermal stability. Microporous and Mesoporous Materials. 2003;**64**:203-211

[92] Landau MV, Dafa E, Kaliya ML, Sen T, Herskowitz M. Mesoporous alumina catalytic material prepared by grafting wide-pore MCM-41 with an alumina multilayer. Microporous and Mesoporous Materials. 2001;**49**:65-81

[93] Passos AR, Martins L, Pulcinelli SH, Santilli CV, Briois V. Effect of the balance between Co(II) and Co(0) oxidation states on the catalytic activity of cobalt catalysts for ethanol steam reforming. Catalysis Today. 2014;**229**:88-94

[94] Pairojpiriyakul T, Croiset E, Kiatkittipong W, Kiatkittipong K, Arpornwichanop A, Assabumrungrat S. Hydrogen production from catalytic supercritical water reforming of glycerol with cobalt-based catalysts. International Journal of Hydrogen Energy. 2013;**38**(11):4368-4379

[95] Chiou JYZ, Lee C-L, Ho K-F, Huang H-H, Yu S-W, Wang C-W. Catalytic performance of Pt-promoted cobalt-based catalysts for the steam reforming of ethanol. International Journal of Hydrogen Energy. 2014;**39**(11):5653-5662

[96] Garbarino G, Riani P, Lucchini MA, Canepa F, Kawale S, Busca G. Cobalt-based nanoparticles as catalysts for low temperature hydrogen production by ethanol steam reforming. International Journal of Hydrogen Energy. 2013;**38**(1):82-91

[97] Papadopoulou E, Delimaris D, Denis A, Machocki A, Ioannides T. Alcohol reforming on cobalt-based catalysts prepared from organic salt precursors. International Journal of Hydrogen Energy. 2012;**37**(21):16375-16381

[98] Llorca J. Efficient production of hydrogen over supported cobalt catalysts from ethanol steam reforming. Journal of Catalysis. 2002;**209**(2):306-317

[99] Busca G, Costantino U, Montanari T, Ramis G, Resini C, Sisani M. Nickel versus cobalt catalysts for hydrogen production by ethanol steam reforming: Ni-Co-Zn-Al catalysts from hydrotalcite-like precursors. International Journal of Hydrogen Energy. 2010;**35**(11):5356-5366

[100] Chen L, Choong CKS, Zhong Z, Huang L, Wang Z, Lin J. Support and alloy effects on activity and product selectivity for ethanol steam reforming over supported nickel cobalt catalysts. International Journal of Hydrogen Energy. 2012;**37**(21):16321-16332

[101] Resini C, Concepción Herrera Delgado M, Presto S, Alemany LJ, Riani P, Marazza R, et al. Yttria-stabilized zirconia (YSZ) supported Ni-Co alloys (precursor of SOFC anodes) as catalysts for the steam reforming of ethanol. International Journal of Hydrogen Energy. 2008;**33**(14):3728-3735

[102] Pereira EB, de la Piscina PR, Homs N. Efficient hydrogen production from ethanol and glycerol by vapour-phase reforming processes with new cobalt-based catalysts. Bioresource Technology. 2011;**102**(3):3419-3423

[103] de la Peña O'Shea VA, Nafria R, Ramírez de la Piscina P, Homs N. Development of robust Co-based catalysts for the selective H_2-production by ethanol steam-reforming. The Fe-promoter effect. International Journal of Hydrogen Energy. 2008;**33**(13):3601-3606

[104] Casanovas A, Roig M, de Leitenburg C, Trovarelli A, Llorca J. Ethanol steam reforming and water gas shift over Co/ZnO catalytic honeycombs doped with Fe, Ni, Cu, Cr and Na. International Journal of Hydrogen Energy. 2010;**35**(15):7690-7698

[105] Xiong H, Motchelaho MAM, Moyo M, Jewell LL, Coville NJ. Cobalt catalysts supported on a micro-coil carbon in Fischer-Tropsch synthesis: A comparison with CNTs and CNFs. Catalysis Today. 2013;**214**:50-60

[106] Xiong H, Zhang Y, Liew K, Li J. Ruthenium promotion of Co/SBA-15 catalysts with high cobalt loading for Fischer-Tropsch synthesis. Fuel Processing Technology. 2009;**90**(2):237-246

[107] Griboval-Constant A, Butel A, Ordomsky VV, Chernavskii PA,

Khodakov AY. Cobalt and iron species in alumina supported bimetallic catalysts for Fischer-Tropsch reaction. Applied Catalysis A: General. 2014;**481**:116-126

[108] Martínez AN, López C, Márquez F, Díaz I. Fischer-Tropsch synthesis of hydrocarbons over mesoporous Co/SBA-15 catalysts: The influence of metal loading, cobalt precursor, and promoters. Journal of Catalysis. 2003;**220**(2):486-499

[109] Wu H, Yang Y, Suo H, Qing M, Yan L, Wu B, et al. Effect of TiO_2 promotion on the structure and performance of silica-supported cobalt-based catalysts for Fischer-Tropsch synthesis. Journal of Molecular Catalysis A: Chemical. 2014;**390**:52-62

[110] Davari M, Karimi S, Tavasoli A, Karimi A. Enhancement of activity, selectivity and stability of CNTs-supported cobalt catalyst in Fischer-Tropsch via CNTs functionalization. Applied Catalysis A: General. 2014;**485**:133-142

[111] Parnian MJ, Taheri Najafabadi A, Mortazavi Y, Khodadadi AA, Nazzari I. Ru promoted cobalt catalyst on γ-Al_2O_3: Influence of different catalyst preparation method and Ru loadings on Fischer-Tropsch reaction and kinetics. Applied Surface Science. 2014;**313**:183-195

[112] Cook KM, Perez HD, Bartholomew CH, Hecker WC. Effect of promoter deposition order on platinum-, ruthenium-, or rhenium-promoted cobalt Fischer-Tropsch catalysts. Applied Catalysis A: General. 2014;**482**:275-286

[113] Karolewska M, Truszkiewicz E, Mierzwa B, Kępiński L, Raróg-Pilecka W. Ammonia synthesis over cobalt catalysts doped with cerium and barium. Effect of the ceria loading. Applied Catalysis A: General. 2012;**445-446**:280-286

[114] Karolewska M, Truszkiewicz E, Wściseł M, Mierzwa B, Kępiński L, Raróg-Pilecka W. Ammonia synthesis over a Ba and Ce-promoted carbon-supported cobalt catalyst. Effect of the cerium addition and preparation procedure. Journal of Catalysis. 2013;**303**:130-134

[115] Campa MC, Luisetto I, Pietrogiacomi D, Indovina V. The catalytic activity of cobalt-exchanged mordenites for the abatement of NO with CH_4 in the presence of excess O_2. Applied Catalysis B: Environmental. 2003;**46**(3):511-522

[116] Campa MC. Catalytic activity of Co-ZSM-5 for the abatement of NOx, with methane in the presence of oxygen. Applied Catalysis B: Environmental. 1996;**8**:315-331

[117] Yan Y, Wang L, Zhang H. Catalytic combustion of volatile organic compounds over Co/ZSM-5 coated on stainless steel fibers. Chemical Engineering Journal. 2014;**255**:195-204

[118] Ulla MA, Lombardo E, Daniell W, Knözinger H. Catalytic combustion of methane on Co/MgO: Characterisation of active cobalt sites. Applied Catalysis B: Environmental. 2001;**29**:217-229

[119] Jiang Z, Yu J, Cheng J, Xiao T, Jones MO, Hao Z, et al. Catalytic combustion of methane over mixed oxides derived from Co-Mg/Al ternary hydrotalcites. Fuel Processing Technology. 2010;**91**(1):97-102

[120] Hunde ET, Watkins JJ. Reactive deposition of cobalt and nickel films from their metallocenes in supercritical carbon dioxide solution. Chemistry of Materials. 2004;**16**(3):498-503

[121] Voorhoeve RJH, Stuiver JCM. The mechanism of the hydrogenation of cyclohexene and benzene on nickel-tungsten sulfide catalysts. Journal of Catalysis. 1971;**23**(2):243-252

[122] Bang Y, Han SJ, Seo JG, Youn MH, Song JH, Song IK. Hydrogen production by steam reforming of liquefied natural gas (LNG) over ordered mesoporous nickel-alumina catalyst. International Journal of Hydrogen Energy. 2012;**37**(23):17967-17977

[123] Majewski AJ, Wood J, Bujalski W. Nickel-silica core@shell catalyst for methane reforming. International Journal of Hydrogen Energy. 2013;**38**(34):14531-14541

[124] Han SJ, Bang Y, Yoo J, Seo JG, Song IK. Hydrogen production by steam reforming of ethanol over mesoporous Ni-Al_2O_3-ZrO_2 xerogel catalysts: Effect of nickel content. International Journal of Hydrogen Energy. 2013;**38**(20):8285-8292

[125] Bimbela F, Oliva M, Ruiz J, García L, Arauzo J. Hydrogen production via catalytic steam reforming of the aqueous fraction of bio-oil using nickel-based coprecipitated catalysts. International Journal of Hydrogen Energy. 2013;**38**(34):14476-14487

[126] Morlanés N. Reaction mechanism of naphtha steam reforming on nickel-based catalysts, and FTIR spectroscopy with CO adsorption to elucidate real active sites. International Journal of Hydrogen Energy. 2013;**38**(9):3588-3596

[127] Nieva MA, Villaverde MM, Monzón A, Garetto TF, Marchi AJ. Steam-methane reforming at low temperature on nickel-based catalysts. Chemical Engineering Journal. 2014;**235**:158-166

[128] Hashemnejad SM, Parvari M. Deactivation and regeneration of nickel-based catalysts for steam-methane reforming. Chinese Journal of Catalysis. 2011;**32**(1):273-279

[129] Lua AC, Wang HY. Decomposition of methane over unsupported porous nickel and alloy catalyst. Applied Catalysis B: Environmental. 2013;**132-133**:469-478

[130] Abelló S, Berrueco C, Montané D. High-loaded nickel-alumina catalyst for direct CO_2 hydrogenation into synthetic natural gas (SNG). Fuel. 2013;**113**:598-609

[131] Lovell E, Jiang Y, Scott J, Wang F, Suhardja Y, Chen M, et al. CO_2 reforming of methane over MCM-41-supported nickel catalysts: Altering support acidity by one-pot synthesis at room temperature. Applied Catalysis A: General. 2014;**473**:51-58

[132] Zhang L, Li L, Zhang Y, Zhao Y, Li J. Nickel catalysts supported on MgO with different specific surface area for carbon dioxide reforming of methane. Journal of Energy Chemistry. 2014;**23**(1):66-72

[133] Tao K, Shi L, Ma Q, Wang D, Zeng C, Kong C, et al. Methane reforming with carbon dioxide over mesoporous nickel-alumina composite catalyst. Chemical Engineering Journal. 2013;**221**:25-31

[134] Fukuhara C, Hyodo R, Yamamoto K, Masuda K, Watanabe R. A novel nickel-based catalyst for methane dry reforming: A metal honeycomb-type catalyst prepared by sol-gel method and electroless plating. Applied Catalysis A: General. 2013;**468**:18-25

[135] Ranjbar A, Rezaei M. Preparation of nickel catalysts supported on $CaO.2Al_2O_3$ for methane reforming with carbon dioxide. International Journal of Hydrogen Energy. 2012;**37**(8):6356-6362

[136] Bereketidou OA, Goula MA. Biogas reforming for syngas production over nickel supported on ceria-alumina catalysts. Catalysis Today. 2012;**195**(1):93-100

[137] Huang L, Zhang F, Chen R, Hsu AT. Manganese-promoted

nickel/alumina catalysts for hydrogen production via auto-thermal reforming of ethanol. International Journal of Hydrogen Energy. 2012;**37**(21):15908-15913

[138] Chan FL, Tanksale A. Review of recent developments in Ni-based catalysts for biomass gasification. Renewable and Sustainable Energy Reviews. 2014;**38**:428-438

[139] Phuhiran C, Takarada T, Chaiklangmuang S. Hydrogen-rich gas from catalytic steam gasification of eucalyptus using nickel-loaded Thai brown coal char catalyst. International Journal of Hydrogen Energy. 2014;**39**(8):3649-3656

[140] Sabatier P, Senderens JB. New synthesis of methane. Comptes Rendus de l'Académie des Sciences. 1902;**134**:514-524

[141] Rahmani S, Rezaei M, Meshkani F. Preparation of promoted nickel catalysts supported on mesoporous nanocrystalline gamma alumina for carbon dioxide methanation reaction. Journal of Industrial and Engineering Chemistry. 2014;**38**(1):118-126

[142] Rahmani S, Rezaei M, Meshkani F. Preparation of highly active nickel catalysts supported on mesoporous nanocrystalline γ-Al_2O_3 for CO_2 methanation. Journal of Industrial and Engineering Chemistry. 2014;**20**(4):1346-1352

[143] Azadi P, Khan S, Strobel F, Azadi F, Farnood R. Hydrogen production from cellulose, lignin, bark and model carbohydrates in supercritical water using nickel and ruthenium catalysts. Applied Catalysis B: Environmental. 2012;**117-118**:330-338

[144] Upare PP, Jeong M-G, Hwang YK, Kim DH, Kim YD, Hwang DW, et al. Nickel-promoted copper-silica nanocomposite catalysts for hydrogenation of levulinic acid to lactones using formic acid as a hydrogen feeder. Applied Catalysis A: General. 2015;**491**:127-135

[145] Peng Q, Spagnola JC, Parsons GN. Self-catalyzed hydrogenolysis of nickelocene: Functional metal coating of three-dimensional nanosystems at low temperature. Journal of the Electrochemical Society. 2008;**155**(9):D580-D582

[146] Bozbag SE, Zhang LC, Aindow M, Erkey C. Carbon aerogel supported nickel nanoparticles and nanorods using supercritical deposition. The Journal of Supercritical Fluids. 2012;**66**:265-273

[147] Taylor AD, DiLeo GJ, Sun K. Hydrogen production and performance of nickel-based catalysts synthesized using supercritical fluids for the gasification of biomass. Applied Catalysis B: Environmental. 2009;**93**(1-2):126-133

[148] Babuněk M, Šimůnek O, Hošek J, Rybáčková M, Cvačka J, Březinová A, et al. Heavy fluorous phosphine-free ruthenium catalysts for alkene metathesis. Journal of Fluorine Chemistry. 2014;**161**:66-75

[149] Liu G, Zhang H, Zhao X, Wang J. Efficient ruthenium metathesis catalysts containing carborane ligands. Journal of Organometallic Chemistry. 2014;**749**:13-17

[150] Gao Y, Jaenicke S, Chuah G-K. Highly efficient transfer hydrogenation of aldehydes and ketones using potassium formate over AlO(OH)-entrapped ruthenium catalysts. Applied Catalysis A: General. 2014;**484**:51-58

[151] Durap F, Aydemir M, Baysal A, Elma D, Ak B, Turgut Y. A new efficient bis(phosphinite)-ruthenium(II) catalyst system for the asymmetric transfer

hydrogenation of aromatic ketones. Inorganica Chimica Acta. 2014;**411**:77-82

[152] Wang Z, Lin J, Wang R, Wei K. Ammonia synthesis over ruthenium catalyst supported on perovskite type $BaTiO_3$. Catalysis Communications. 2013;**32**:11-14

[153] Li Y, Pan C, Han W, Chai H, Liu H. An efficient route for the preparation of activated carbon supported ruthenium catalysts with high performance for ammonia synthesis. Catalysis Today. 2011;**174**(1):97-105

[154] Akbayrak S, Kaya M, Volkan M, Özkar S. Ruthenium(0) nanoparticles supported on magnetic silica coated cobalt ferrite: Reusable catalyst in hydrogen generation from the hydrolysis of ammonia-borane. Journal of Molecular Catalysis A: Chemical. 2014;**394**:253-261

[155] Akbayrak S, Tanyıldızı S, Morkan I, Özkar S. Ruthenium(0) nanoparticles supported on nanotitania as highly active and reusable catalyst in hydrogen generation from the hydrolysis of ammonia borane. International Journal of Hydrogen Energy. 2014;**39**(18):9628-9637

[156] Ma Y, Huang Y, Cheng Y, Wang L, Li X. Biosynthesized ruthenium nanoparticles supported on carbon nanotubes as efficient catalysts for hydrogenation of benzene to cyclohexane: An eco-friendly and economical bioreduction method. Applied Catalysis A: General. 2014;**484**:154-160

[157] Liao H, Ouyang D, Zhang J, Xiao Y, Liu P, Hao F, et al. Benzene hydrogenation over oxide-modified MCM-41 supported ruthenium-lanthanum catalyst: The influence of zirconia crystal form and surface hydrophilicity. Chemical Engineering Journal. 2014;**243**:207-216

[158] Arena BJ. Deactivation of ruthenium catalysts in continuous glucose hydrogenation. Applied Catalysis A: General. 1992;**87**:219-229

[159] Mishra DK, Dabbawala AA, Park JJ, Jhung SH, Hwang J-S. Selective hydrogenation of d-glucose to d-sorbitol over HY zeolite supported ruthenium nanoparticles catalysts. Catalysis Today. 2014;**232**:99-107

[160] Hao C, Wang S, Li M, Kang L, Ma X. Hydrogenation of CO_2 to formic acid on supported ruthenium catalysts. Catalysis Today. 2011;**160**(1):184-190

[161] Yen CH, Lin HW, Tan C-S. Hydrogenation of bisphenol A—Using a mesoporous silica based nano ruthenium catalyst Ru/MCM-41 and water as the solvent. Catalysis Today. 2011;**174**(1):121-126

[162] Kim D, Lee HBR, Yoon J, Kim H. Ru nanodot synthesis using CO_2 supercritical fluid deposition. Journal of Physics and Chemistry of Solids. 2013;**74**(5):664-667

[163] Zhang Y, Jiang H, Wang Y, Zhang M. Synthesis of highly dispersed ruthenium nanoparticles supported on activated carbon via supercritical fluid deposition. Industrial & Engineering Chemistry Research. 2014;**53**(15):6380-6387

[164] Xu S, Li L, Li R, Su Y. Preparation of Ru/C catalysts by supercritical CO_2 deposition. Xiyou Jinshu Cailiao Yu Gongcheng/Rare Metal Materials and Engineering. 2011;**40**(12):2142-2146

[165] Zhao Y, Zhang J, Song J, Li J, Liu J, Wu T, et al. Ru nanoparticles immobilized on metal-organic framework nanorods by supercritical CO_2-methanol solution: Highly efficient catalyst. Green Chemistry. 2011;**13**(8):2078-2082

[166] Szègedi A, Kónya Z, Méhn D, Solymár E, Pál-Borbély G, Horváth ZE,

et al. Spherical mesoporous MCM-41 materials containing transition metals: Synthesis and characterization. Applied Catalysis A: General. 2004;**272**:257-266

[167] Sobczak I, Ziolek M, Nowacka M. Preparation and characterization of Pt containing NbMCM-41 mesoporous molecular sieves addressed to catalytic NO reduction by hydrocarbons. Microporous and Mesoporous Materials. 2005;**78**:103-116

[168] Shanbhag GV, Joseph T, Halligudi SB. Copper(II) ion exchanged AlSBA-15: A versatile catalyst for intermolecular hydroamination of terminal alkynes with aromatic amines. Journal of Catalysis. 2007;**250**:274-282

[169] Brunauer S, Deming LS, Deming WE, Teller E. On a theory of the Van der Waals adsorption of gases. Journal of the American Chemical Society. 1940;**62**:1723-1732

[170] Morey M, Davidson A, Eckert H, Stucky G. Pseudotetrahedral O_3/2VO centers immobilized on the walls of a mesoporous, cubic MCM-48 support: Preparation, characterization and reactivity toward water as investigated by 51V NMR and UV-Vis spectroscopies. Chemistry of Materials. 1996;**8**:486-492

[171] Sing KS, Everett DH, Haul RAW, Moscou L, Pierotti RA, Rouquerol J, et al. Reporting physisorption data for gas/solid systems with special reference to the determination of surface area and porosity. Pure and Applied Chemistry. 1985;**57**:603-619